Atmos. Chem. Phys., 26, 3881–3900, 2026
https://doi.org/10.5194/acp-26-3881-2026

Atmospheric Chemistry and Physics
Open Access
EGU

Assessment and prediction of dust emissions, deposition and radiation forcing in Central Asia

Ying Gan[1,2,3], **Zhe Zhang**[1,2,3,4], **Wen Chu**[5], **Jianli Ding**[6], **and Yuxin Ren**[1,2,3]

[1]College of Geography and Remote Sensing Sciences, Xinjiang University, Urumqi, 830046, China
[2]Xinjiang Key Laboratory of Oasis Ecology, Xinjiang University, Urumqi, 830046, China
[3]Key Laboratory of Smart City and Environment Modelling of Higher Education Institute, Xinjiang University, Urumqi, 830046, China
[4]MNR Technology Innovation Center for Central Asia Geo-Information Exploitation and Utilization, Urumqi, 830046, China
[5]College of Marine Technology, Faculty of Information Science and Engineering, Ocean University of China, Qingdao, 266100, China
[6]Xinjiang Institute of Technology, Aksu, 843100, China

Correspondence: Zhe Zhang (zhangzhe_0110@yeah.net)

Received: 28 February 2025 – Discussion started: 18 June 2025
Revised: 30 January 2026 – Accepted: 20 February 2026 – Published: 19 March 2026

Abstract. Dust aerosols significantly influence climate by modulating radiative balance and cloud processes. This study integrates MERRA-2 reanalysis data and the CMIP6 multi-model ensemble to assess the spatiotemporal evolution of dust emissions, deposition, and associated radiative effects in Central Asia from 1980 to 2100. Four SSP scenarios project that dust emissions in Central Asia exhibit a high-emission, high-deposition pattern with primary sources exceeding $15\,\mu\mathrm{g\,m^{-2}\,s^{-1}}$. The deposition area substantially exceeds the source area (maximum $> 8\,\mu\mathrm{g\,m^{-2}\,s^{-1}}$). Cross-scenario analysis demonstrates that dust emissions are highly sensitive to climate policy, with end-of-century emissions in the SSP5-8.5 high-emission scenario increasing by 94.9 % relative to the baseline period. In contrast, emissions under the SSP1-2.6 low-carbon pathway vary by only 4.5 %. Simulations using the SBDART model show that aerosol direct radiative forcing (ADRF) from dust in Central Asia under clear-sky conditions exhibits a vertical gradient, with cooling at the top of the atmosphere (TOA) and heating within the atmosphere, yielding a net negative forcing at the TOA, with a minimum of $< -10\,\mathrm{W\,m^{-2}}$ near the Caspian Sea. Peak positive forcing within the atmosphere, observed in spring, reaches $10.0\,\mathrm{W\,m^{-2}}$. Increased dust emissions reduce shortwave radiation at the surface by up to $-20\,\mathrm{W\,m^{-2}}$. Ground-based observations indicate seasonal variations in the dust-induced heating rate, with peak radiative forcing in spring at Kashgar ($93.0\,\mathrm{W\,m^{-2}}$) and a maximum near-surface heating rate of $2.6\,\mathrm{K\,d^{-1}}$. In contrast, the near-surface heating rate at Issyk-Kul Lake in autumn ($0.34\,\mathrm{K\,d^{-1}}$) is approximately four times higher than in spring ($0.08\,\mathrm{K\,d^{-1}}$).

1 Introduction

Dust aerosols are a significant component of the tropospheric aerosol mass load, accounting for approximately 50 %, and profoundly impact the functioning of the Earth system (Mahowald et al., 2010; Ramanathan et al., 2001). Their transboundary circulation process (lithosphere-atmosphere-cryosphere) and interaction with the climate system have become cutting-edge research areas in Earth system science. The release, transport, and deposition of dust aerosols not only involve multiple geospheres but also substantially affect weather, climate, air quality, and human health upon entering the atmosphere (Tegen et al., 2004; Penner et al., 2006; Pozzer et al., 2012).

Global annual dust emissions are substantial, ranging from approximately 1000 to 2150 Tg, with 30 % to 40 % originating from arid regions of Asia (Tanaka and Chiba, 2006). Dust is transported across continents by westerly wind circulation, significantly influencing the atmospheric radiation balance in East Asia, North America, and the Arctic region (Wallace and Hobbs, 2006). Although studies have confirmed that dust regulates the land-atmosphere energy budget through direct radiative forcing (including scattering and absorption of shortwave and longwave radiation) and indirect effects (such as altering precipitation efficiency as cloud condensation nuclei), significant uncertainty persists regarding the vertical distribution of dust, the amplification mechanism of anthropogenic emissions, and their regional climate feedback (IPCC, 2021).

Due to the challenges associated with dust observation, our understanding of the behavior of dust throughout its life cycle remains insufficient, hindering a complete understanding and accurate modeling of its complex mechanism of action (Kok et al., 2023; Rupakheti et al., 2023). Numerous studies have used a variety of methods, including in situ observations, satellite remote sensing, and model simulations, to thoroughly examine the spatiotemporal changes, optical properties, and radiative forcing of dust aerosols (Wang et al., 2018; Song et al., 2021; Chen et al., 2022). For example, global dust is primarily confined to the “dust belt”, with approximately one-third originating from the Asian region (Kok et al., 2023). Dai et al. (2022) utilized a variety of remote sensing and ground-based data to study the sources, microphysical characteristics, and optical properties (Dai et al., 2022; Salvador et al., 2022). Zhao et al. (2023) investigated the simulation of global and regional dust by 16 CMIP6 models in the Atmospheric Model Intercomparison Project (AMIP) experiment and compared the results with observational and reanalysis data (Zhao et al., 2023; Liu et al., 2024).

Model simulations provide information on the temporal and spatial changes of dust aerosols worldwide and facilitate predictions of future trends (Li et al., 2021). Climate models, such as CMIP5 and CMIP6, have enhanced our understanding of the main characteristics of dust aerosols. These models feature increasing resolutions and increasingly complex physical processes and parameterizations, demonstrating their ability to simulate dust events and processes on meso- to global scales (Zhao et al., 2022). In particular, CMIP6 experiments have provided critical support for assessing the climatic effects of dust emissions (Braconnot et al., 2021; Zhao et al., 2024). However, due to insufficient resolution and simplified regional topography, the applicability of these global studies to the arid regions of Central Asia remains limited, underscoring the need for high-resolution analyses at the regional scale.

The arid regions of Central Asia, including Xinjiang in China, constitute the world’s second-largest dust source area, with distinctive surface characteristics leading to significant spatiotemporal variations in dust emission fluxes (Shen et al., 2016). However, current research has primarily focused on the spatiotemporal distribution and transport processes of dust (Li et al., 2022b; Tao et al., 2022), while key aspects of the local dust lifecycle in this region – such as the long-term evolution of dust emission–deposition budgets, the strong dependence of direct radiative forcing on dust vertical profiles, and modal differences in dust–climate feedbacks under different carbon emission scenarios – remain poorly understood. These knowledge gaps significantly constrain the reliability of climate models over Central Asia, and uncertainties in radiative forcing estimates primarily stem from the lack of ground-based validation due to the scarcity of observational stations (Brown et al., 2021; Wu and Boor, 2021).

To overcome the above limitations, this study establishes a multi-source data integration framework that systematically incorporates a full-chain analysis of “emission–deposition–radiation”, focusing on the regional characteristics of the dust lifecycle over the arid regions of Central Asia. Unlike previous studies that have mainly concentrated on the global scale (Kok et al., 2023; Zhao et al., 2022, 2023, 2024), this work achieves an integrated assessment at the regional scale and emphasizes the role of observations in constraining model uncertainties. The specific innovations are reflected in three aspects: (1) by combining MERRA-2 reanalysis with CMIP6 multi-model ensembles through statistical downscaling, the long-term evolution of dust emission–deposition budgets and their scenario-based differences in Central Asia are systematically characterized, thereby providing regionally refined insights to complement global model results; (2) using the SBDART radiative transfer model together with observational data from the SONET Asian Dust Monitoring Network and the Jinghe CE318 ground-based remote sensing site, the long-term trends of dust shortwave radiative forcing under clear-sky conditions are quantified; and (3) by introducing the SARIMA statistical model, the short-term evolution and risk implications of dust radiative effects are explored. This framework not only deepens the understanding of dust physical mechanisms under the complex topography and local climate of Central Asia but also provides new scientific support for improving regional climate simulations and environmental risk management.

The structure of this paper is as follows. Section 2 presents the data sources, the downscaling method for the CMIP6 dust budget, and the calculation method for clear-sky aerosol radiative forcing. Section 3 examines the detailed characteristics of the dust budget, projections of future changes, and the radiative forcing of dust aerosols. Finally, the main conclusions and a discussion are presented in Sect. 4.

2 Data and Methods

2.1 Data sources

The study area is situated between 35–57° N and 48–96° E, encompassing the five Central Asian countries (Kazakhstan, Uzbekistan, Tajikistan, Turkmenistan, and Kyrgyzstan) and the Xinjiang region of China (comprising both its northern

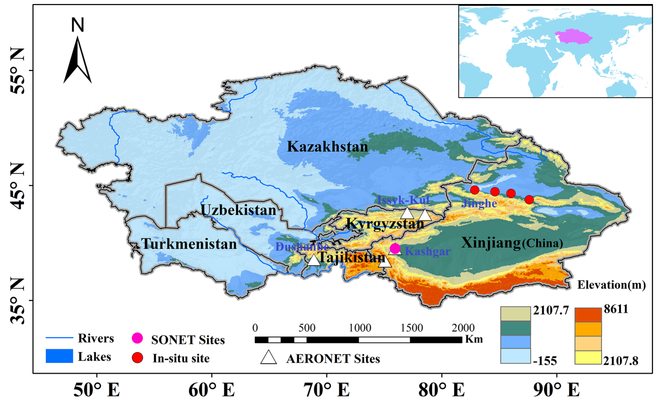

Figure 1. Location of the study area.

and southern parts) (Fig. 1). This region, located in the hinterland of the Eurasian continent, is characterized by a temperate continental climate with extreme aridity. The region features a highly heterogeneous surface, with the Taklamakan Desert and the surrounding Gobi (comprising over 40 % of the study area) interspersed with mountain ranges, such as the Tianshan and Pamir, forming a unique landform (Hetzel et al., 2002; Shen et al., 2016). As the world's second-largest source of dust, strong thermal and dynamic coupling drives intense dust activities (Zhang et al., 2020), with emission hotspots concentrated in the Tarim Basin, the desiccated bed of the Aral Sea, and the Kazakh steppe belt. This study focuses on the regional dust budget and radiative effects, utilizing MERRA-2 reanalysis data, the CMIP6 multi-model ensemble, AERONET, SONET, and handheld photometer data.

2.1.1 Ground-based sun photometer data

AERONET (AErosol RObotic NETwork) employs a CE-318 solar photometer to measure aerosol optical depth (AOD) across eight bands in the range of 340–1640 nm and to derive microphysical parameters, including single scattering albedo (SSA), refractive index (m), and particle size spectrum (Holben et al., 1998; Holben et al., 2001). The Level 2 data exhibit an uncertainty of less than 5 %. As an internationally recognized standard for ground-based aerosol observations, its long-term stability and algorithmic consistency provide reliable input for radiative forcing calculations (García et al., 2012). The data used in this study are available from the AERONET website (https://aeronet.gsfc.nasa.gov/, last access: 4 March 2026).

The Chinese Academy of Sciences-led SONET (Sun-sky radiometer Observation NETwork) employs the CE318-DP instrument to provide information on the chemical composition and vertical profile of aerosols while adhering to AERONET's stringent quality control procedures. The establishment of SONET sites has effectively addressed gaps in AERONET's spatial coverage in this source region (Li et al., 2018). Cross-validation demonstrates that the correlation coefficient between SONET and AERONET AOD is 0.98 (RMSE < 0.02), confirming a seamless integration of the two datasets (She et al., 2024). The SONET data can be accessed from its official website (https://spaceclimateobservatory.aerss.net/, last access: 10 March 2026).

To supplement the limited temporal and spatial coverage of fixed stations, this study employs CE-318 and Microtops II handheld photometers to obtain transient AOD observations in the 550–870 nm band (accuracy ± 0.01) for verifying the local applicability of satellite inversion products. By integrating these multi-scale observational data, this study uses AERONET and SONET Level 2 data to provide vertical profiles of aerosol optical-physical properties, calculate the direct radiative forcing of aerosols, and validate satellite data on AOD and radiation flux in Central Asia (Supplement Fig. S1).

2.1.2 MERRA-2 reanalysis data

The MERRA-2 reanalysis data used in this study was developed by NASA's Goddard Space Flight Center. Its core is based on the GEOS-5 atmospheric circulation model and the ADAS-5.12.4 assimilation system. A global multi-element dataset with 72 vertical layers (surface to 80 km) and a horizontal resolution of $0.625° \times 0.5°$ has been constructed from 1980 to the present by integrating satellite remote sensing (MODIS/AVHRR aerosol optical thickness), ground-based observations (soundings, aircraft observations), and GOCART aerosol chemical transport model output (Gelaro et al., 2017). In addition to covering variables related to clouds, radiation, and hydrological cycles, the coupled GOCART model distinguishes the interaction mechanisms of five aerosol types in this dataset: dust (DU), sea salt (SS), sulfate (SO4), black carbon (BC), and organic carbon (OC). For the first time, the entire lifecycle of dust aerosols has been analyzed, providing key parameters such as monthly average dust emission flux, dry/wet deposition rate, particle size-classified loads, and single scattering albedo at 483.5 nm, ensuring physical consistency for quantifying dust radiative forcing (Buchard et al., 2017). Leveraging these data advantages, this study extracts radiation flux and dust cycle parameters under clear-sky conditions in Central Asia and systematically constructs a collaborative analysis framework for dust emissions, deposition, and radiative forcing.

2.1.3 CMIP6 model simulations

The Sixth Coupled Model Intercomparison Project (CMIP6) incorporates 112 climate models from 33 institutions worldwide, with its multi-scenario simulations substantially exceeding those of previous studies in both breadth and depth (Eyring et al., 2016). To examine the decadal variations in dust emissions and dry and wet deposition in Central Asia, this study selected ten models from CMIP6 based on data completeness. The selection criteria encompassed key variables in the dust cycle: monthly mean dust emission fluxes for the historical period (1980–2014) and for four Shared Socioeconomic Pathways (SSP1-2.6, SSP2-4.5, SSP3-7.0, and SSP5-8.5) from 2015 to 2100, as well as dust dry- and wet-deposition fluxes (the sum of which constitutes total deposition).

To ensure spatial consistency when comparing multi-source data, all model outputs were statistically downscaled and regridded to match the MERRA-2 reanalysis data (spatial resolution: 0.625° × 0.5°). This multi-model ensemble approach effectively captures uncertainties in climate responses while managing computational costs, thereby providing robust data support for analyzing the long-term evolution of the dust cycle in the arid region of Central Asia.

2.2 Methodology

2.2.1 Delta statistical downscaling

Due to the limited original spatial resolution of the CMIP6 models (typically $\sim 1.25° \times 1°$), their direct application to regional-scale dust cycle analyses may introduce systematic biases. Therefore, this study employs the delta change factor method for statistical downscaling. At its core, this method separates the historical biases of the climate models from the future change signal, enabling the reconstruction of high-resolution climate variables (Maraun et al., 2010; Gutmann et al., 2014).

First, deviations during the baseline period are calculated by extracting the monthly mean dust emission fluxes, $P_{\mathrm{m,his}}$, from the historical simulations (1980–2014) of each CMIP6 model. These fluxes are then matched to the MERRA-2 reanalysis observations, P_{obs}, for the same period to determine the model's systematic deviation ratio.

$$B_{\mathrm{m}} = \frac{P_{\mathrm{m,his}}}{\overline{P}_{\mathrm{obs}}} \tag{1}$$

where $\overline{P}_{\mathrm{obs}}$ is the monthly average of the observation period, and B_{m} represents the spatial deviation of model m in the reference period.

Second, the relative change factor for future scenarios is extracted, and the ratio of dust emissions for each model during the future scenario period (2015–2100) relative to its historical simulation is calculated.

$$R_{\mathrm{m,fut}} = \frac{P_{\mathrm{m,fut}}}{\overline{P}_{\mathrm{m,his}}} \tag{2}$$

Among them, $P_{\mathrm{m,fut}}$ is the monthly mean emission of model m in the future, and $P_{\mathrm{m,his}}$ is the monthly mean emission of model m over the historical period.

This approach decouples the historical deviations from the climate change signal, preserving the physical response characteristics of CMIP6 to future climate forcings while enhancing simulation accuracy at the regional scale through the incorporation of high-resolution observational data. Compared

Table 1. Overview of the models and simulations used in this study.

Model	Nation	Resolution	Hist	SSP126	SSP245	SSP370	SSP585	Dust emission scheme	Model references
CESM2-WACCM	USA	1.25° × 0.94°	3	1	5	3	5	Zender et al. (2003)	Danabasoglu et al. (2020)
CESM2	USA	1.25° × 0.95°	11	3	3	3	3	Zender et al. (2003)	Wu et al. (2016)
CNRM-ESM2-1	France	1.25° × 0.96°	3	5	10	5	5	Marticorena et al. (1997)	Séférian et al. (2019)
GFDL-ESM4	USA	1.25° × 0.97°	1	1	1	1	1	Evans et al. (2016)	Dunne et al. (2020)
GISS-E2-1-G	USA	1.25° × 0.98°	19	10	25	17	10	Miller et al. (2004)	Bauer et al. (2020)
GISS-E2-1-H	USA	1.25° × 0.99°	10	5	5	1	5	Bauer and Koch (2005)	Kelley et al. (2020)
GISS-E2-2-G	USA	1.25° × 1.00°	5	5	5	5	5	Cakmur et al. (2006)	Rind et al. (2020)
MRI-ESM2-0	Japan	1.25° × 1.01°	12	5	10	5	6	Tanaka and Chiba.(2005)	Yukimoto et al. (2019)
HadGEM3-GC31-LL	UK	1.875° × 1.25°	5	3	4	2	3	Marticorena and Bergametti (1995)	Kuhlbrodt et al. (2018)
UKESM1-0-LL	UK	1.25° × 1.875°	3	5	5	3	4	Marticorena and Bergametti (1995)	Senior et al. (2020)

to dynamic downscaling, it substantially reduces computational costs and is particularly suitable for multi-model uncertainty quantification studies.

2.2.2 SBDART Radiative Transfer Model Calculation of Direct Radiative Forcing of Aerosols

The Santa Barbara DISORT Atmospheric Radiative Transfer (SBDART) model (Ricchiazzi et al., 1998) was employed in this study to quantitatively assess the direct radiative effects of aerosols. SBDART solves the atmospheric radiative transfer equation using the four-stream approximation. Its core architecture comprises three modules: first, the discrete ordinates radiative transfer (DISORT) module, which calculates the radiative fluxes in a 45-layer atmosphere (with a vertical resolution of 0.3 km); second, the spectral parameterization module, which integrates the LOWTRAN-7 atmospheric absorption spectrum and Mie scattering theory to cover the shortwave band from 0.25 to 4.0 µm; and third, the surface-atmosphere coupling module, which analyzes the radiative interactions between surface albedo and atmospheric constituents such as water vapor and ozone.

This study is based on a comprehensive dataset, with key input parameters including the optical properties (e.g., optical depth τ, single scattering albedo ω, asymmetry factor g) and the vertical profiles of aerosols. These parameters were obtained from the solar photometer observation network in Central Asia, which provides significant advantages in temporal and spatial resolution compared to satellite retrieval products (Dubovik and King, 2000). To quantify the radiative forcing due to dust aerosols, all simulations were conducted under clear-sky conditions, with the solar zenith angle fixed to the seasonal mean value for the study area to ensure the comparability of regional radiative effects (Halthore et al., 2005). The aerosol direct radiative forcing (ADRF) was calculated using the standard approach, which determines the difference in net radiative flux with and without aerosols under cloud-free conditions. Specifically, the ADRF at a given altitude z, at the top of the atmosphere (TOA), at the surface (SFC), and in the atmosphere (ATM) can be defined as follows:

$$\mathrm{NF}_z = F_{z,\mathrm{down}} - F_{z,\mathrm{up}} \tag{3}$$

$$\mathrm{ADRF}_z = \mathrm{NF}_z^{\mathrm{aer}} - \mathrm{NF}_z^{\mathrm{noaer}} \tag{4}$$

$$\mathrm{ADRF}_{\mathrm{TOA}} = \mathrm{NF}_{\mathrm{TOA}}^{\mathrm{aer}} - \mathrm{NF}_{\mathrm{TOA}}^{\mathrm{noaer}} \tag{5}$$

$$\mathrm{ADRF}_{\mathrm{SFC}} = \mathrm{NF}_{\mathrm{SFC}}^{\mathrm{aer}} - \mathrm{NF}_{\mathrm{SFC}}^{\mathrm{noaer}} \tag{6}$$

$$\mathrm{ADRF}_{\mathrm{ATM}} = \mathrm{ADRF}_{\mathrm{TOA}} - \mathrm{ADRF}_{\mathrm{SFC}} \tag{7}$$

$$\mathrm{ADRF}_{\mathrm{dust}} = \mathrm{ADRF} \times \left(\frac{\mathrm{DAOD}}{\mathrm{AOD}}\right) \tag{8}$$

Among them, $F_{z,\mathrm{down}}$ and $F_{z,\mathrm{up}}$ are the downward and upward radiative fluxes, $\mathrm{NF}_z^{\mathrm{aer}}$ and $\mathrm{NF}_z^{\mathrm{noaer}}$ are the net radiative fluxes with and without aerosols, and ADRF is the aerosol direct radiative forcing.

2.2.3 SARIMA prediction model

Given the non-stationarity and interannual cycle characteristics of the radiative forcing time series of Central Asian dust, this study employs the seasonal autoregressive integrated moving average (SARIMA) model for analysis. First, the augmented Dickey-Fuller test (ADF, $p<0.05$) was used to confirm the non-stationarity of the series. A compound differencing strategy (first-order conventional difference $d=1$, first-order seasonal difference $D=1$, period $s=12$) was applied to eliminate trend and interannual fluctuations, resulting in a stationary residual series (KPSS test, $p>0.1$).

The non-seasonal order ($p=2$, $q=1$) was determined based on the autocorrelation function (ACF) and partial autocorrelation function (PACF), while the seasonal order ($P=1$, $Q=1$) was optimized using grid search, yielding the final $\mathrm{SARIMA}(2,1,1)(1,1,1)_{12}$ model (AIC = 112.3, BIC = 125.7). Model validation demonstrated a goodness of fit of $R^2=0.87$ for annual cycle dynamics, with a prediction error for extreme event peaks of less than 15 %, confirming its effectiveness in analyzing non-stationary sequences (Sirisha et al., 2022).

2.2.4 Linear Trend Method

In this study, the ordinary least squares (OLS) method was used to perform linear regression on the dust budget time series, with trend significance assessed via a two-tailed t-test. Spatial trends were derived by conducting independent regressions at each grid point, with statistically significant results ($p<0.05$) indicated by stippling in the figures. Regional mean trends were calculated by regressing the annual averages of grid values within specific regions (Central Asian countries, northern Xinjiang, and southern Xinjiang). The regression slopes and corresponding p-values were annotated directly on the time series plots.

3 Results and Analysis

3.1 Spatial pattern and multi-mode prediction of dust emissions in Central Asia

Figure 2 compares MERRA-2 observations with CMIP6 multi-model ensemble (MME) dust emissions from 1980 to 2014. The historical spatial distribution from the 10 models is shown in Fig. S2. Further analysis indicates that the observations are highly consistent with the MME simulations, yielding a Taylor skill score (SS) of 0.87 and demonstrating strong performance in both correlation and standard deviation. Dust emissions in the study area exhibit substantial temporal and spatial variability. In terms of spatial distribution (Fig. 2a), both datasets consistently identify the three primary core emission sources in the Tarim Basin, the desiccated Aral Sea bed, and the Gobi Desert, with maximum emission fluxes exceeding 15 $\mu\mathrm{g\,m^{-2}\,s^{-1}}$. Regarding the trends in dust emissions (Fig. 2b), those in the Aral Sea region have increased significantly ($> 0.5\,\mu g\,m^{-2}\,s^{-1}\,yr^{-1}$) over the past 34 years, whereas those in the Tarim Basin have slightly decreased ($\approx -0.3\,\mu g\,m^{-2}\,s^{-1}\,yr^{-1}$).

The Aral Sea region has experienced a 68 % reduction in lake area since 1960, resulting in 54 000 km^2 of exposed lakebed (Wang et al., 2020). Under arid climatic conditions – with annual average precipitation of less than 100 mm and potential evaporation exceeding 2000 mm – the dust emission flux has increased significantly at a rate of approximately $0.5\,\mu g\,m^{-2}\,s^{-1}\,yr^{-1}$ over 34 years. In contrast, the Tarim Basin has benefited from ecological restoration projects and increased precipitation during the growing season (Fu et al., 2021), leading to a decrease in emission flux at a rate of $\approx -0.3\,\mu g\,m^{-2}\,s^{-1}\,yr^{-1}$. Time series analysis (Fig. 2c) shows that overall dust emissions fluctuate gently without significant annual trends. Dust emissions in the southern Tarim Basin of Xinjiang exhibit annual increases and decreases, consistent with the spatial trend distribution. Dust emissions in northern Xinjiang are similar to those in Central Asia, with northern Xinjiang slightly higher than other Central Asian regions. This may be attributed to local differences in surface roughness and land use, reflecting regional disparities in emission characteristics.

In the future projections, Fig. 3 illustrates the relative changes in dust emissions over Central Asia under four radiative forcing scenarios (SSP1-2.6, SSP2-4.5, SSP3-7.0, and SSP5-8.5) for the near term (2021–2040), midterm (2051–2070), and long term (2081–2100), relative to the baseline period (1980–2014). The results reveal pronounced spatiotemporal heterogeneity in dust emissions across the region (absolute values are shown in Fig. S7). Under all scenarios, regions with high dust emission values (changes $> 10\,\mu g\,m^{-2}\,s^{-1}$ and relative change rates $> 25\,\%$) are consistently located in the Aral Sea basin, Turkmenistan, and the eastern margin of the Tarim Basin. Overall, dust emission intensity shows a positive correlation with the magnitude of radiative forcing and increases progressively over time within each scenario (long term > midterm > near term). Specifically, in the Aral Sea region, near-term dust emissions range from $17.8\,\mu g\,m^{-2}\,s^{-1}$ (SSP3-7.0) to $26.0\,\mu g\,m^{-2}\,s^{-1}$ (SSP2-4.5), with relatively small inter-scenario differences. However, as radiative forcing intensifies and time progresses, the rate of change in emissions rises from approximately 40 % in the near term to about 70 % in the midterm. Under the high-radiative-forcing scenario (SSP5-8.5), the long-term increase reaches its maximum, with an enhancement of about 94.9 % relative to the reference period.This substantial increase is closely associated with the exposure of saline–alkaline sediments from the desiccated lakebed, soil loosening due to rising surface temperatures, and intensified wind erosion (Lioubimtseva and Cole, 2006).

In contrast, the Tarim Basin exhibits an overall decreasing trend in dust emissions, primarily driven by the combined effects of ecological restoration (a decadal NDVI increase of 0.12) and enhanced growing-season precipitation (Xu et al., 2019). Specifically, dust emissions decline by 18.7 % under SSP2-4.5 and by 29.3 % under SSP3-7.0. Under the SSP5-8.5 scenario, emissions decrease from $27.2\,\mu g\,m^{-2}\,s^{-1}$ in the near term to $20.1\,\mu g\,m^{-2}\,s^{-1}$ in the long term, representing a reduction of approximately 26.1 %, with the relative change rate showing a concurrent weakening trend.A regional comparison reveals substantial differences in climate response sensitivity: the emission increases over the Aral Sea region exhibit an exponential relationship with radiative forcing intensity ($R^2 = 0.93$), whereas those in southern Xinjiang show a slight declining tendency. This contrast highlights the potential role of human interventions in modulating dust processes across Central Asia.

Dust emissions and deposition together constitute the complete dust mass balance process, with deposition representing the ultimate outcome of dust release. Once injected into the atmosphere, dust particles undergo dry deposition, driven primarily by gravitational settling, and wet deposition, facilitated by precipitation (the historical spatial distributions of dry and wet deposition from the ten models are shown in Figs. S3–S4), thereby completing the material redistribution across the land–atmosphere interface (Marticorena and Bergametti, 1995; Shao et al., 2011). Quantitative assessments (Figs. 4 and 5–6) indicate that the multi-model ensemble (MME) simulations agree well with observations in reproducing total dust deposition over Central Asia, yielding a Taylor skill score of 0.82. However, differences exist in the absolute magnitudes of deposition, and the observed trend intensity from MERRA-2 is substantially stronger than that simulated by the model ensemble. Spatially, regions with high deposition ($> 5\,\mu g\,m^{-2}\,s^{-1}$) largely coincide with emission hotspots, mainly concentrated in western Central Asia and the Tarim Basin in southern Xinjiang, confirming the spatially coupled "emission–deposition" mechanism of local dust processes. Trend analysis (Fig. 4b) reveals that the Aral Sea and the eastern Caspian region exhibit the strongest positive trends ($\Delta S = +0.15\,\mu g\,m^{-2}\,s^{-1}$), whereas southern Xinjiang is dominated by a negative trend ($\Delta S = -0.10\,\mu g\,m^{-2}\,s^{-1}$). Temporally (Fig. 4c), the observational data show a slight increasing trend in dust deposition flux over Central Asia during 1980–2014, with a rate of $0.002\,\mu g\,m^{-2}\,s^{-1}\,yr^{-1}$, while the MME simulations indicate a weak decreasing trend of $-0.003\,\mu g\,m^{-2}\,s^{-1}\,yr^{-1}$ over Xinjiang. This discrepancy between observations and simulations may stem from uncertainties in model representations of boundary-layer dynamics and precipitation microphysics in arid Central Asia, particularly in the quantification of dust wet deposition efficiency, which still requires improvement.

Figure 5 illustrates the projected relative changes in dust deposition under four SSP scenarios across different time periods (future changes in dry and wet deposition are shown in Figs. S9–S10). Unlike the source-concentrated distribution of dust emissions, the spatial extent of deposition extends outward, mainly covering south-

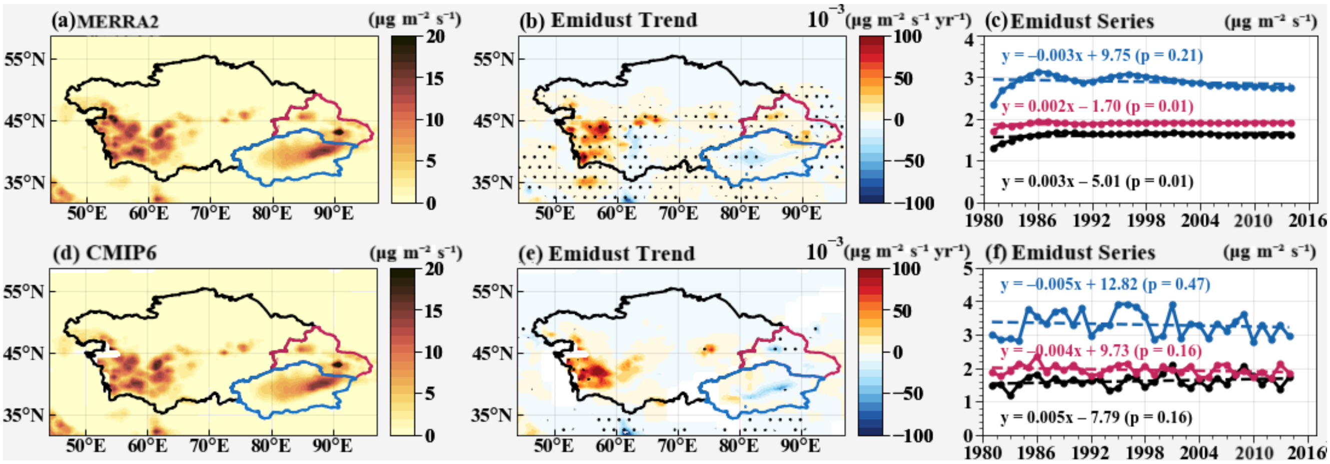

Figure 2. Spatial distribution, linear trends, and time series of dust emissions from MERRA-2 and the CMIP6 multi-model ensemble (MME) in Central Asia from 1980 to 2014. The red outline delineates Northern Xinjiang, the blue outline delineate Southern Xinjiang, and the black outlines denote the five Central Asian countries. Black dots in panels **(b)** and **(e)** mark regions significant at the 95 % confidence level.

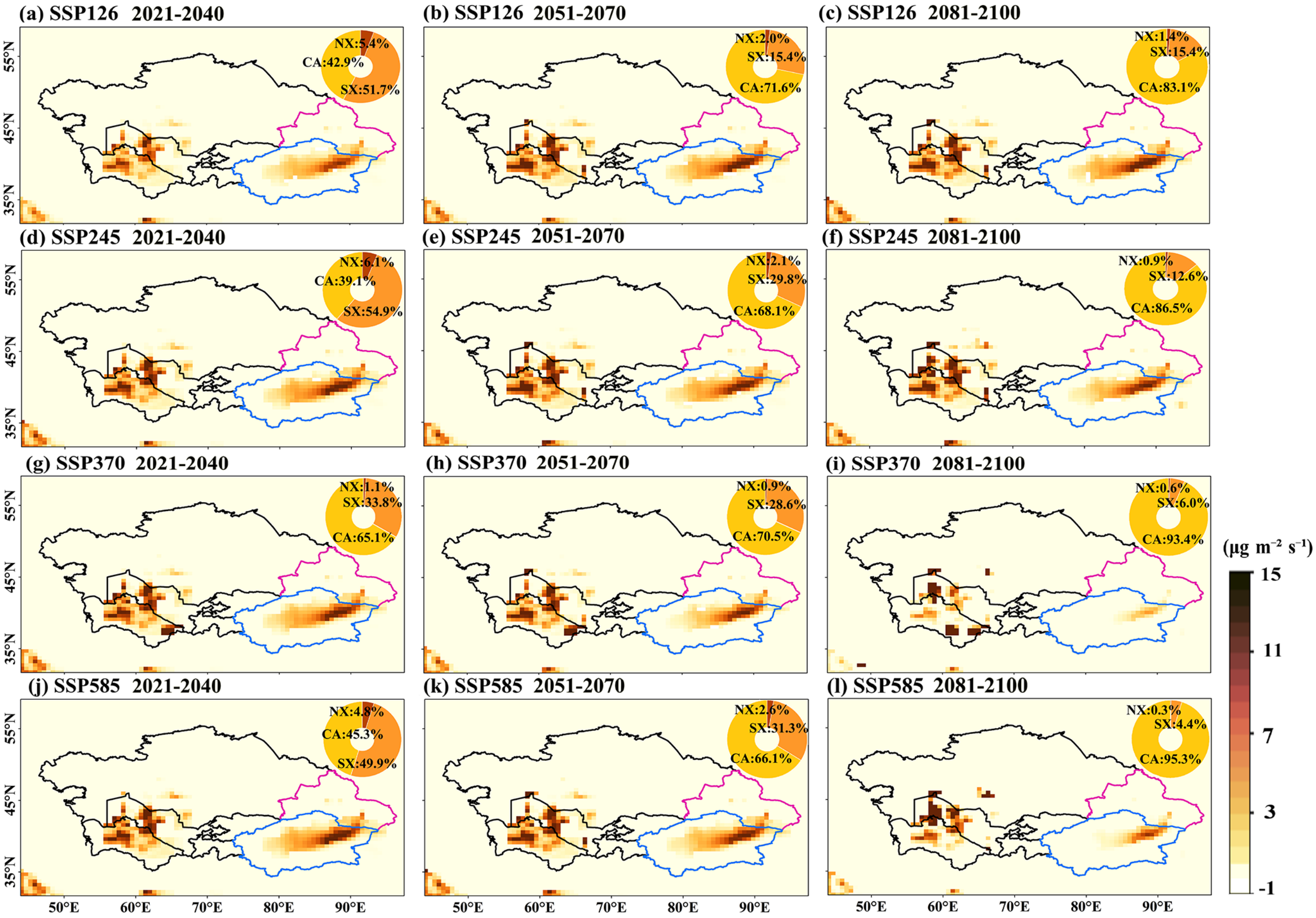

Figure 3. Future changes in dust emissions across different periods. Spatial distribution of the relative changes in dust emissions over Central Asia under four CMIP6 multi-model ensemble (MME) SSP scenarios: **(a–d)** near term (2021–2040), **(e–h)** midterm (2051–2070), and **(i–l)** long term (2081–2100), relative to the historical period (2000–2014). The circular inset in the upper-right corner of each panel indicates the mean relative change rate (%) for the corresponding region.

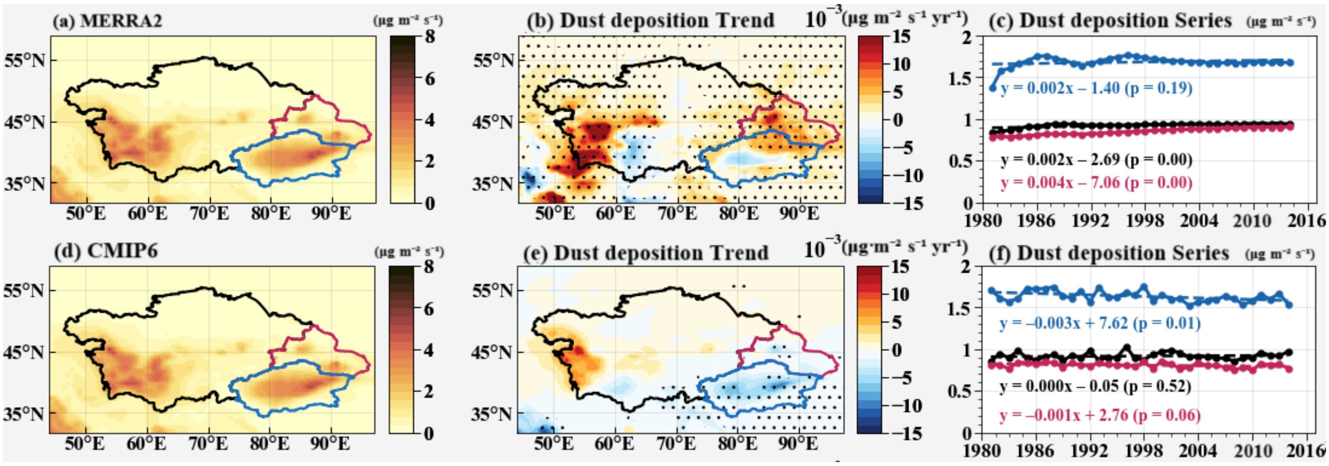

Figure 4. Spatial distribution, linear trends, and temporal variations of total dust deposition (dry + wet) over Central Asia from 1980 to 2014, based on MERRA-2 observations and CMIP6 multi-model ensemble (MME) simulations. Red shading highlights northern Xinjiang, blue shading indicates southern Xinjiang, and black outlines denote the five Central Asian countries. In panels **(b)** and **(e)**, black dots denote regions where the trends are statistically significant at the 95 % confidence level ($p < 0.05$).

western Central Asia, the southeastern margin of the Tarim Basin, and the Junggar Basin, with maximum deposition fluxes exceeding 8 $\mu g\,m^{-2}\,s^{-1}$. This forms a distinct spatial pattern characterized by a "deposition domain > emission source". From a temporal perspective, near-term (2021–2040) mean deposition ranges from 9.3 $\mu g\,m^{-2}\,s^{-1}$ (SSP5-8.5) to 10.4 $\mu g\,m^{-2}\,s^{-1}$ (SSP2-4.5), whereas long-term (2081–2100) values vary between 9.6 $\mu g\,m^{-2}\,s^{-1}$ (SSP3-7.0) and 10.0 $\mu g\,m^{-2}\,s^{-1}$ (SSP1-2.6). The overall change is less than 1 $\mu g\,m^{-2}\,s^{-1}$, corresponding to a variation amplitude below 12 %, and the relative change rate remains stable across all scenarios, suggesting that future radiative forcing exerts limited influence on dust deposition processes.This phenomenon may be attributed to the compensatory effects between dry and wet deposition. In southern Xinjiang, changes in the precipitation regime under moderate-to-high radiative forcing lead to a gradual decline in dry deposition flux at a rate of approximately 0.2 $\mu g\,m^{-2}\,s^{-1}\,yr^{-1}$. Conversely, in western Central Asia, enhanced near-surface wind speeds resulting from reduced surface roughness increase dry deposition, while the spatiotemporal stability of wet deposition mitigates fluctuations in total deposition.

To more accurately assess the trend simulation performance of the dust cycle, we constructed time series of dust emissions and wet and dry deposition from 1980 to 2100 based on MERRA-2 reanalysis data and CMIP6 multi-model ensemble (MME) simulations (see Fig. 6). Overall, the simulations indicate that dust emissions in Xinjiang remain relatively stable over the next 120 years. In contrast, in the five Central Asian countries – particularly under high-radiative-forcing scenarios (e.g., SSP3-7.0, SSP5-8.5) – dust emissions increase significantly (e.g., up to 94.9 % under SSP5-8.5) between 2081 and 2100, accompanied by a fluctuating but gradual rise. By comparison, dust deposition (both dry and wet) exhibits a smoother trend with lower volatility.

In the specific analyses, MERRA-2 dust emissions show a smooth trend, with averages of 30 $\mu g\,m^{-2}\,s^{-1}$ in the Tarim Basin and 15 $\mu g\,m^{-2}\,s^{-1}$ in other regions. In contrast, MME-simulated emissions exhibit slight fluctuations, with peaks exceeding 45 $\mu g\,m^{-2}\,s^{-1}$ at certain times. Some deviations are observed in the temporal variability between the two datasets. The volatility of dust dry deposition is relatively low, with a slope of less than 0.1, indicating a smooth process. Additionally, neither dry nor wet deposition shows significant long-term volatility. Wet deposition exhibits slight deviations in northern Xinjiang but remains relatively smooth in other regions, with an average flux of approximately 1.5 $\mu g\,m^{-2}\,s^{-1}$ and an overall slope of less than 0.2, indicating limited variation. Notably, MERRA-2 wet deposition data show a marked increase in the northern border region around 2000, likely related to the assimilation of MODIS satellite and other observations in MERRA-2. Therefore, MERRA-2 data from 2000 to 2014 were selected for model calibration to ensure simulation accuracy. In summary, although future dust emissions vary substantially under different climate scenarios, the overall dust deposition process remains relatively stable. The MERRA-2 and MME simulation results exhibit spatial and temporal differences across regions.

3.1.1 Monthly average changes in direct radiative forcing by dust aerosols

Based on the quantitative characterization of dust emission sources and deposition processes described above, further investigation is needed to elucidate the perturbation mechanisms of dust aerosols on the surface–atmosphere

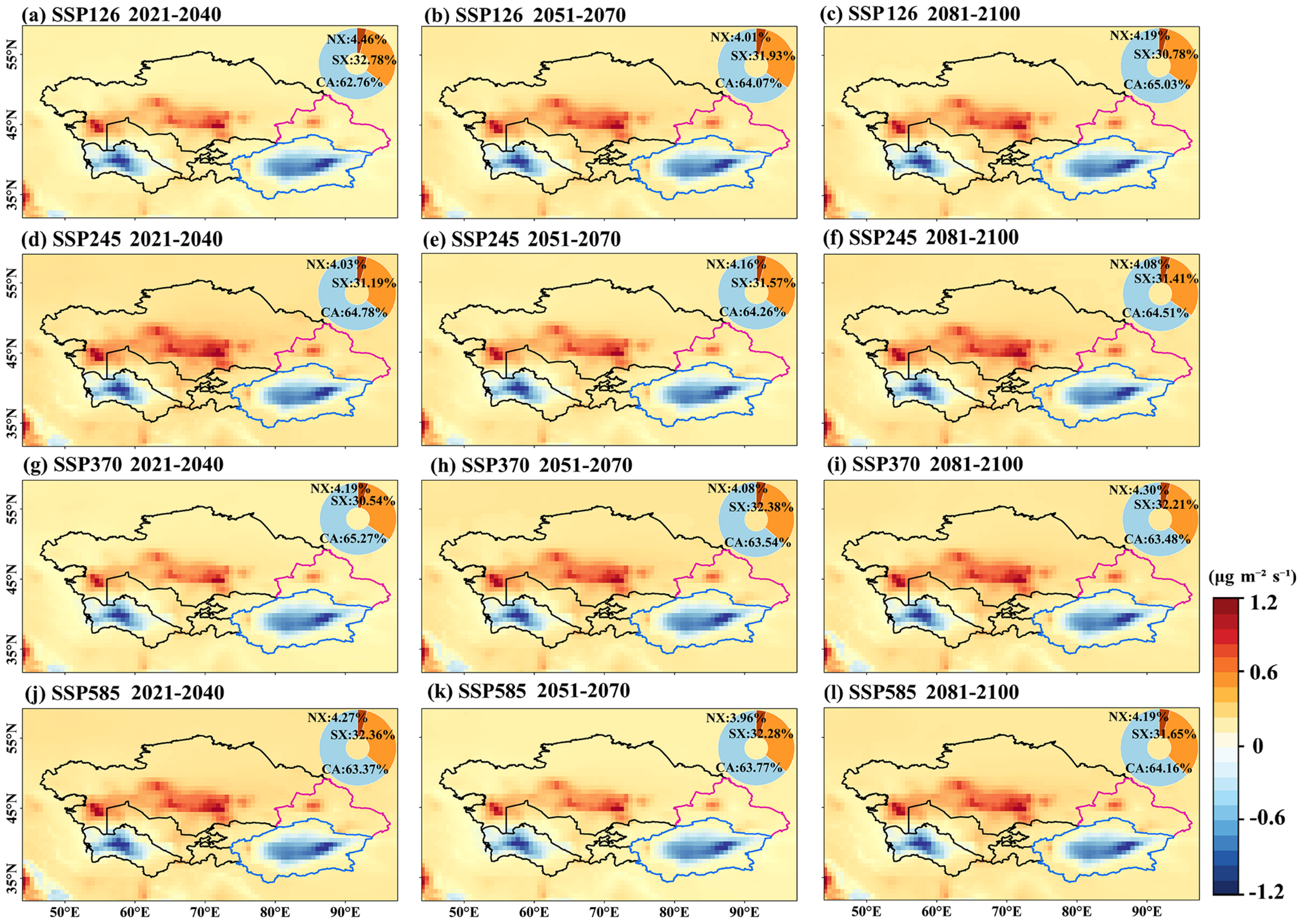

Figure 5. Spatial distribution of relative changes in total dust deposition over Central Asia under four CMIP6 multi-model ensemble (MME) SSP scenarios for different future periods: **(a–d)** near term (2021–2040), **(e–h)** midterm (2051–2070), and **(i–l)** long term (2081–2100), relative to the historical period (2000–2014). The circular inset in the upper-right corner of each panel indicates the mean relative change rate (%) for the corresponding region.

energy balance. This study quantifies the radiative impacts of Central Asian dust aerosols at various spatial and temporal scales through shortwave aerosol direct radiative forcing (ADRF) derived from MERRA-2 observations under clear-sky conditions from 1980 to 2023. As shown in Fig. 7a–d, the top-of-atmosphere (TOA) radiative forcing exhibits substantial spatial heterogeneity. Overall, the negative forcing reaches its lowest values ($< -10\,\mathrm{W\,m^{-2}}$) in the Caspian Sea region, followed by the Tarim Basin and the Aral Sea region ($< -8\,\mathrm{W\,m^{-2}}$), confirming that dust aerosols exert a significant cooling effect by enhancing shortwave reflection. Seasonal analysis reveals that the negative TOA forcing intensity decreases in the order spring ($-3.32\,\mathrm{W\,m^{-2}}$) > summer ($-3.21\,\mathrm{W\,m^{-2}}$) > autumn ($-3.07\,\mathrm{W\,m^{-2}}$) > winter ($-1.94\,\mathrm{W\,m^{-2}}$), which aligns closely with the seasonal characteristics of dust activity. In spring, strong surface wind erosion across Central Asia drives intense dust emissions, resulting in high atmospheric dust loading and optical depth and, consequently, the strongest radiative forcing. Although summer convective activity can transport dust to higher altitudes, weakened near-surface wind erosion reduces the overall dust burden relative to spring (Ginoux et al., 2012). During autumn and winter, dust activity declines markedly, yielding the weakest annual radiative forcing.

The spatial pattern of surface (SFC) radiative forcing (Fig. 7e–h) exhibits stronger negative values, with two pronounced cooling centers over the Tarim Basin and southwestern Central Asia, where shortwave radiation loss peaks at $-20\,\mathrm{W\,m^{-2}}$. This arises from the combined scattering and absorption effects of dust particles on incoming solar radiation (Li et al., 2022a), which substantially reduce surface net radiation, thereby diminishing sensible heat flux and evaporation processes and suppressing the transfer of heat and water vapor from the surface to the atmosphere. The atmospheric radiative forcing (ADRF) exhibits a spatial pattern consistent with those at the TOA and SFC but features positive values ($10.02\,\mathrm{W\,m^{-2}}$ in spring and $9.89\,\mathrm{W\,m^{-2}}$ in

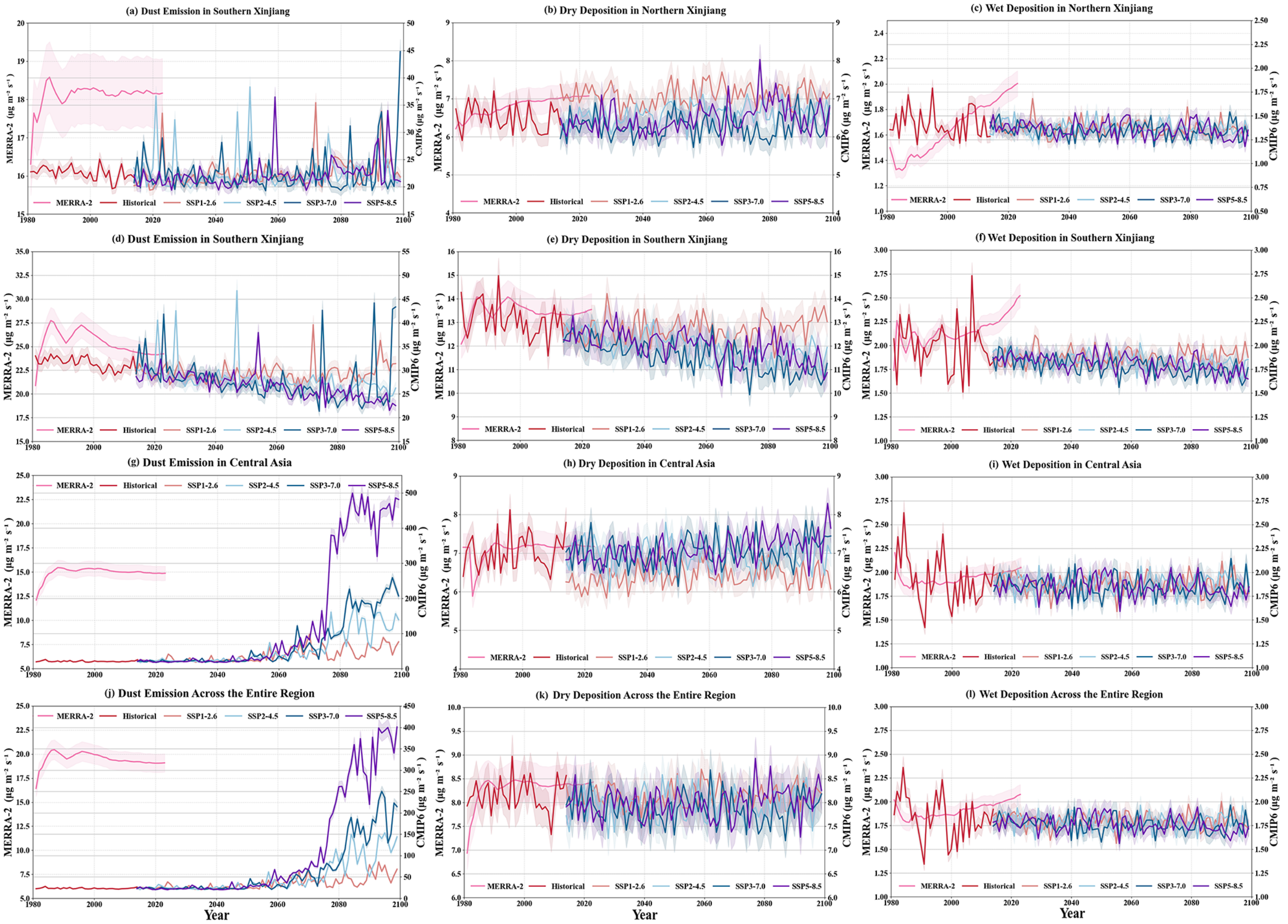

Figure 6. Time evolution of the dust budget. Dust emissions, dry and wet deposition ($\mu g\,m^{-2}\,s^{-1}$) for **(a–c)** Northern Xinjiang, **(d–f)** Southern Xinjiang, **(g–i)** Central Asia, and **(j–l)** the entire study region. Results are from the CMIP6 multi-model ensemble (MME; 1980–2100) and MERRA-2 (1980–2023).

summer), indicating the energy redistribution role of dust aerosols in trapping solar energy within the atmospheric system via shortwave absorption.This vertical gradient of "surface cooling and atmospheric heating" induces substantial changes in the regional thermodynamic structure (Kok et al., 2017). On one hand, surface cooling diminishes sensible heat flux and evaporation, thereby exacerbating moisture deficits in Central Asia's arid regions and limiting vegetation growth and agricultural productivity. On the other hand, atmospheric heating strengthens the temperature gradient from the boundary layer to the free troposphere, enhancing the potential for deep convection, which could intensify the frequency and severity of spring–summer dust storms and modify regional precipitation patterns and extreme weather events.

3.1.2 Refinement of aerosol direct radiative forcing in dusty weather

Following a thorough examination of the spatial distribution characteristics of atmospheric dust aerosol direct radiative forcing (DRF) derived from MERRA-2 reanalysis data, this study further refines the analysis by simulating the radiative effects of dust aerosols at representative Central Asian sites using the Santa Barbara DISORT Atmospheric Radiative Transfer (SBDART) model (Fig. 8).

These simulations are based on ground-based observations from 2011 to 2023, encompassing AERONET sites at Dushanbe (Tajikistan; representing the Central Asian interior), Issyk-Kul (Kyrgyzstan; representing high-altitude lake regions), and Kashgar (Xinjiang, China; representing the Tarim Basin dust source region), as well as the SONET site at Kashgar and our self-established Jinghe site (Xinjiang, China; representing the Gobi–desert transitional zone). Although the number of sites is limited, their spatial distribution covers the primary dust source regions and represen-

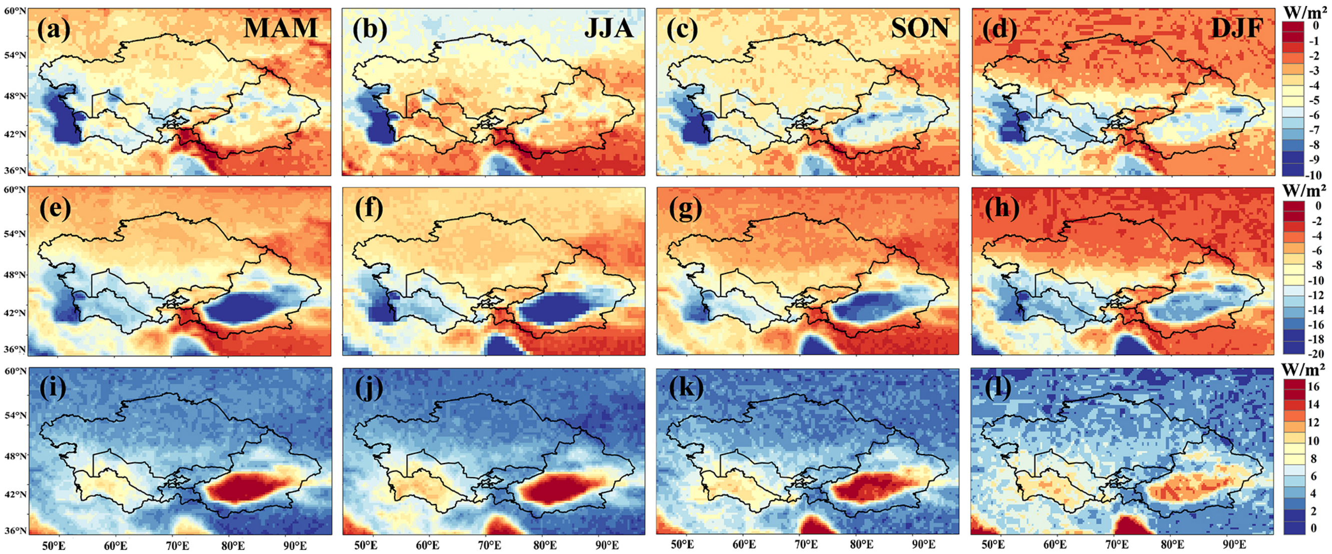

Figure 7. Seasonal spatial distribution of clear-sky shortwave aerosol direct radiative forcing (ADRF) due to dust aerosols in Central Asia (1980–2023): at the top of the atmosphere **(a–d)**, at the surface **(e–h)**, and in the atmosphere **(i–l)**.

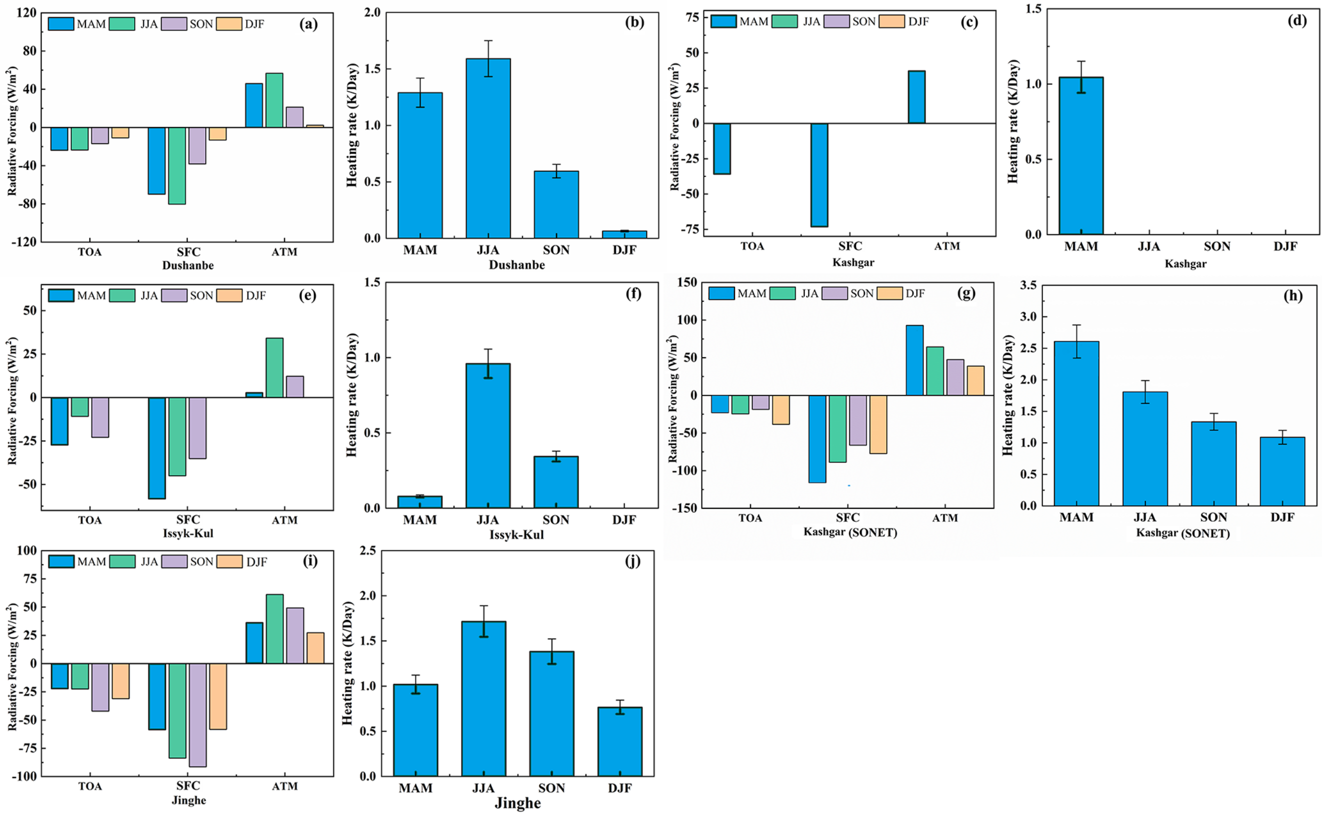

Figure 8. Seasonally averaged shortwave radiative forcing and atmospheric heating rate (including direct radiative forcing at the top of the atmosphere (TOA), the surface (SUR), and the atmosphere (ATM)) for dust aerosols at stations in Central Asia.

tative surface types, thereby achieving a degree of regional representativeness.This section focuses on site-scale aerosol direct radiative forcing (ADRF), with particular emphasis on atmospheric radiative forcing (ATM) and the associated atmospheric heating rates, to provide a detailed understanding of the thermodynamic effects of dust on the atmospheric column.

Observations indicate that ADRF exhibits distinct seasonal variations. At the Dushanbe, Issyk-Kul, and Jinghe sites, atmospheric radiative forcing peaks in summer (56.72, 34.22, and 61.17 $\mathrm{W\,m^{-2}}$, respectively) and declines to annual minima in winter (approximately 2.33 $\mathrm{W\,m^{-2}}$ at Dushanbe and 27.36 $\mathrm{W\,m^{-2}}$ at Jinghe), consistent with the frequent summer dust events in western Central Asia driven by westerly circulation (Li et al., 2022b).Notably, the Kashgar site exhibits a unique spring-dominated pattern, with a maximum ADRF of 92.99 $\mathrm{W\,m^{-2}}$, which may be associated with the Tarim Basin's specific dust emission mechanisms, involving springtime snowmelt that exposes bare surfaces and interacts with intense Mongolian cyclone activity.

Changes in the atmospheric heating rate maintain a clear positive correlation with ADRF, confirming the central role of radiation absorption by dust aerosols. The peaks in heating rates at all sites occur during the active dust period: those at Dushanbe (1.29 $\mathrm{K\,d^{-1}}$ in summer) and Jinghe (1.72 $\mathrm{K\,d^{-1}}$ in summer) align with westerly transport paths, while the anomalously high value at Kashgar in spring (2.61 $\mathrm{K\,d^{-1}}$) corresponds to significant sand uplift events in the Taklamakan Desert. Notably, the heating rate at Issyk-Kul in spring (0.08 $\mathrm{K\,d^{-1}}$) is substantially lower than that in autumn (0.34 $\mathrm{K\,d^{-1}}$), possibly due to the site being shielded by mountainous terrain, which limits vertical dust transport in spring. This may also affect the accuracy of the results, given the relative scarcity of observational data at the Issyk-Kul site.This study reveals that the spatial and temporal divergence of regional radiative effects is primarily controlled by two major factors: (1) seasonal modulation of emission intensity in dust source regions, exemplified by enhanced dust transport from westerly jets to the Aral Sea basin in summer, and (2) modulation of localized atmospheric boundary layer processes, typically manifested as differences in thermal response between a mountainous site (Issyk-Kul) and a basin site (Kashgar). These findings provide essential observational constraints for improving dust-radiation parameterization schemes in regional climate models.

Figure 9 provides a further refinement of the aerosol direct radiative forcing (ADRF) at the sites, revealing that the daily variations in radiative forcing at the top of the atmosphere (TOA), surface (SFC), and throughout the atmosphere exhibit a clear pattern of temporal divergence. The ADRF time series at each site shows a differentiated response: at Dushanbe (2011–2023), typical characteristics of inland Central Asia are evident, with TOA and SFC forcing oscillating within ±200 $\mathrm{W\,m^{-2}}$ and atmospheric heating rates peaking at 8 $\mathrm{K\,d^{-1}}$. Short-term variations are primarily driven by intermittent dust transport induced by disturbances in the westerly jet. At the Jinghe site, a generally stable trend is observed, punctuated by transient episodes of strong negative forcing (SFC $< -250\,\mathrm{W\,m^{-2}}$) during extreme dust events. The Kashgar site displays pronounced temporal variability, with TOA/SFC forcing ranging from $\pm 400\,\mathrm{W\,m^{-2}}$ and heating rates between 0 and 8 $\mathrm{K\,d^{-1}}$ during 2016–2022, including high-frequency oscillations in the afternoons of spring and summer. This behavior is directly linked to the Tarim Basin's unique "afternoon mixed-layer development–vertical dust uplift" mechanism (Nakamae and Takemi, 2022), which may further increase the likelihood of regional dust events by intensifying local convective activity.

Notably, recent observations indicate enhanced irregular variability in ADRF during 2020–2023, which may be attributed to the combined effects of changing surface cover and the increased frequency of extreme weather events in arid Central Asia, resulting in heightened instability in dust emissions and boundary-layer thermodynamic responses. At Kashgar, pronounced day-to-day fluctuations ($\Delta\mathrm{ADRF} > 50\,\mathrm{W\,m^{-2}}$) reveal the sensitive feedback of aerosol loading from the Taklamakan Desert source region on boundary-layer thermodynamics.These high-resolution observational results suggest that transient perturbations in dust radiative effects may alter boundary-layer stability and convective potential, thereby influencing precipitation variability and ecosystem stability in arid Central Asia. Such findings provide critical observational constraints for dust–radiation parameterizations in regional climate models.

4 Conclusion and discussion

4.1 Conclusion

Dust aerosols play a pivotal role in the climate system, characterized by substantial complexity and regional variability. This study compares the spatial distributions and temporal trends of dust emissions and deposition in Central Asia, while projecting future trends based on MERRA-2 reanalysis data and dust cycle simulations from the CMIP6 multi-model ensemble (MME). Comparative analysis from 1980 to 2014 reveals strong consistency between the reanalysis data and MME simulations. The primary dust emission hotspots are the Tarim Basin, the desiccated Aral Sea region, and the Gobi Desert, where maximum emission fluxes exceed 15 $\mathrm{\mu g\,m^{-2}\,s^{-1}}$. Over the 34-year period, dust emissions in the Aral Sea region have increased significantly ($> 0.5\,\mathrm{\mu g\,m^{-2}\,s^{-1}\,yr^{-1}}$), whereas emission fluxes in the Tarim Basin exhibit a declining trend at a rate of $\approx -0.3\,\mathrm{\mu g\,m^{-2}\,s^{-1}\,yr^{-1}}$.

Regarding short-, medium-, and long-term projections, regions with high dust emission values in Central Asia remain stable in the Aral Sea hinterland, Turkmenistan, and along the eastern margin of the Tarim Basin. Short-term emissions in the Aral Sea region range from 17.8 to 26.0 $\mathrm{\mu g\,m^{-2}\,s^{-1}}$,

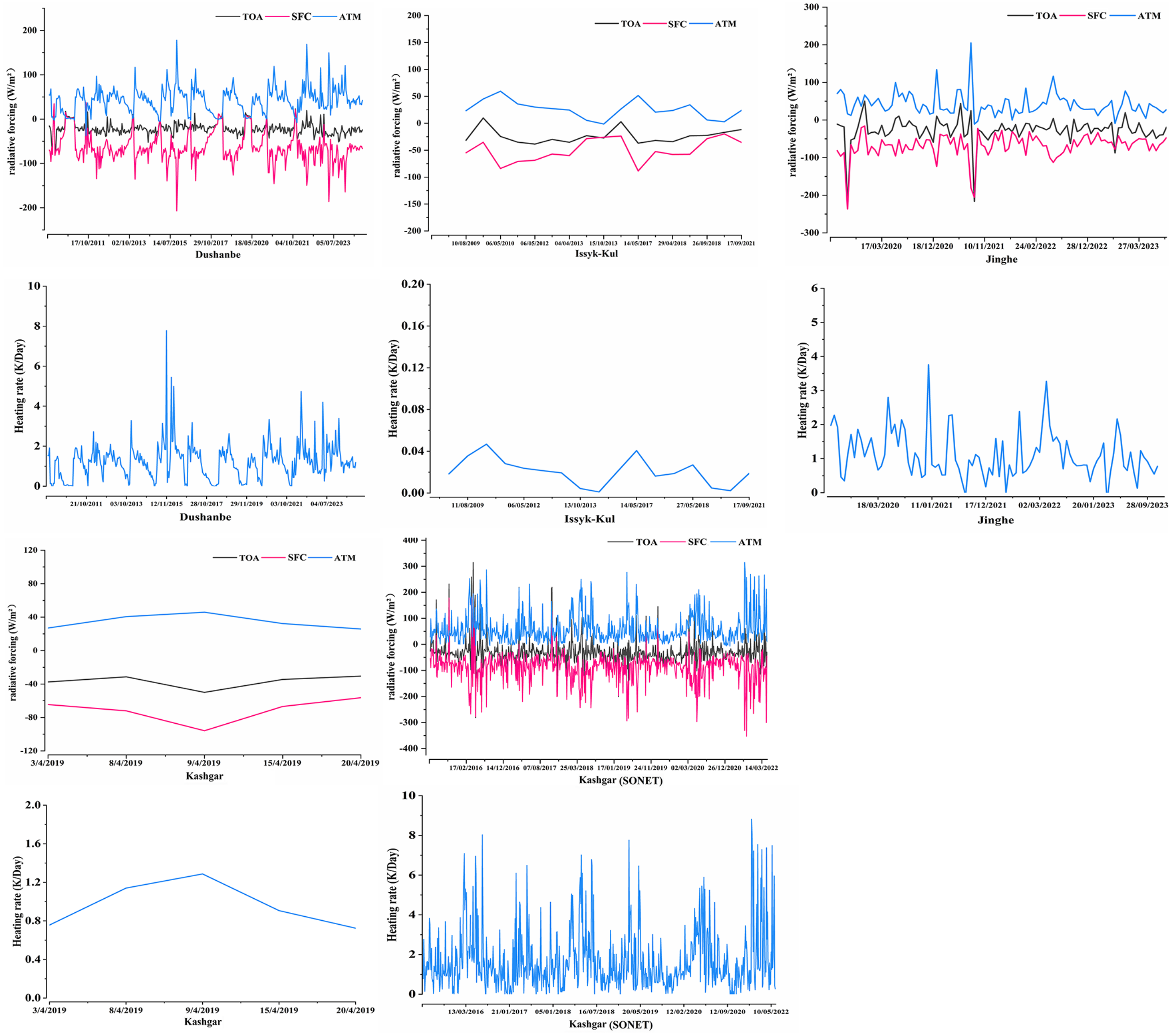

Figure 9. Shortwave direct radiative forcing and atmospheric heating rates at Central Asian sites (AERONET/SONET data). **(a)**, **(b)**, **(c)**, **(g)**, **(h)** show forcing at the top of the atmosphere (TOA), surface (SFC), and in the atmosphere (ATM); **(d)**, **(e)**, **(f)**, **(i)**, **(j)** show the corresponding atmospheric heating rates for **(a, d)** Dushanbe, **(b, e)** Issyk-Kul, **(c, f)** Jinghe, and **(g–j)** Kashgar.

exhibiting minimal inter-scenario variation; however, under high-radiative-forcing scenarios (e.g., SSP5-8.5), long-term dust emissions in Central Asia increase to 387.1 $\mu g\,m^{-2}\,s^{-1}$, representing an enhancement of up to 94.9 % relative to the reference period. In contrast, long-term emissions in the Tarim Basin demonstrate a declining trend, with reductions ranging from 18.7 % under the SSP2-4.5 scenario to 29.3 % under the SSP3-7.0 scenario. Particularly under the SSP5-8.5 scenario, short-term emissions stand at 27.2 $\mu g\,m^{-2}\,s^{-1}$, decreasing to 20.1 $\mu g\,m^{-2}\,s^{-1}$ in the long term – a reduction of 26.1 %.

Regions with high dust deposition values ($> 5\,\mu g\,m^{-2}\,s^{-1}$) overlap substantially with emission hotspots. Trend analysis reveals that the Aral Sea and the eastern Caspian region exhibit the strongest positive trends ($\Delta S = +0.15\,\mu g\,m^{-2}\,s^{-1}$), whereas southern Xinjiang shows a negative trend ($\Delta S = -0.10\,\mu g\,m^{-2}\,s^{-1}$). Under the four future scenarios, dust deposition influences extend across southwestern Central Asia, the southeastern margin of the Tarim Basin, and the Junggar Basin, with maximum fluxes exceeding 8 $\mu g\,m^{-2}\,s^{-1}$. Mean values in the near term (2021–2040) range from 9.3 $\mu g\,m^{-2}\,s^{-1}$ (SSP5-8.5) to 10.4 $\mu g\,m^{-2}\,s^{-1}$ (SSP2-4.5), and from 9.6 $\mu g\,m^{-2}\,s^{-1}$ (SSP3-7.0) to

$10.0\,\mu\mathrm{g\,m^{-2}\,s^{-1}}$ (SSP1-2.6) in the long term (2081–2100), with an overall variation of less than 12 %.

The aerosol direct radiative forcing (ADRF) due to dust aerosols under clear skies in Central Asia exhibits notable spatial patterns. Overall, the top-of-atmosphere (TOA) radiative forcing is negative, with the lowest values observed in the Caspian Sea region ($< -10\,\mathrm{W\,m^{-2}}$), followed by the Tarim Basin and the Aral Sea region ($< -8\,\mathrm{W\,m^{-2}}$). The seasonal TOA forcing minima decrease in the order spring ($-3.32\,\mathrm{W\,m^{-2}}$) > summer ($-3.21\,\mathrm{W\,m^{-2}}$) > autumn ($-3.07\,\mathrm{W\,m^{-2}}$) > winter ($-1.94\,\mathrm{W\,m^{-2}}$). At the surface (SFC), radiative forcing reaches a peak of $-20\,\mathrm{W\,m^{-2}}$ in the Tarim Basin and southwestern Central Asia. Atmospheric shortwave radiative forcing aligns spatially with TOA and SFC patterns, peaking at $10.02\,\mathrm{W\,m^{-2}}$ in spring, which correlates closely with the seasonal characteristics of dust activity.

Simulations using the SBDART model indicate that aerosol direct radiative forcing (ADRF) at the sites peaks in summer at Dushanbe ($56.72\,\mathrm{W\,m^{-2}}$), Issyk-Kul ($34.22\,\mathrm{W\,m^{-2}}$), and Jinghe ($61.17\,\mathrm{W\,m^{-2}}$), declining to annual minima in winter (approximately $2.33\,\mathrm{W\,m^{-2}}$ at Dushanbe and $27.36\,\mathrm{W\,m^{-2}}$ at Jinghe). At Kashgar, ADRF exhibits a distinct spring peak of $92.99\,\mathrm{W\,m^{-2}}$. Variations in atmospheric heating rates show a strong positive correlation with ADRF. Heating rate peaks occur during the active dust season at all sites: summer at Dushanbe ($1.29\,\mathrm{K\,d^{-1}}$) and Jinghe ($1.72\,\mathrm{K\,d^{-1}}$), and spring at Kashgar ($2.61\,\mathrm{K\,d^{-1}}$). Notably, the heating rate at Issyk-Kul is substantially lower in spring (0.08 K/day) than in autumn ($0.34\,\mathrm{K\,d^{-1}}$), reflecting seasonal modulation of dust emission intensity and the influence of local boundary layer processes.

4.2 Discussion

4.2.1 SARIMA Forecasting

This study integrates MERRA-2 reanalysis data, CMIP6 multi-model ensemble (MME) simulations, and ground-based sun photometer observations to develop a fully coupled "emission–deposition–radiation" framework for the dust cycle in Central Asia, thereby systematically elucidating the radiative regulatory mechanisms of dust aerosols on the land–atmosphere system. To address the pronounced spatiotemporal heterogeneity in aerosol radiative forcing and the limitations of observational data, this study employs a seasonal autoregressive integrated moving average (SARIMA) model. Leveraging MERRA-2 reanalysis data and SBDART-derived site-level radiative forcing time series from 1980 to 2023, this approach facilitates short-term predictive analyses from local to regional scales.

In contrast to century-scale CMIP6 scenario simulations, the SARIMA model quantifies the interannual and short-term internal variability in dust radiative forcing (Kumar et al., 2018), enabling operational forecasts for the next 5–10 years. This method is particularly well-suited for near-term predictions of high-uncertainty variables, as it effectively captures seasonal and short-term fluctuations while providing quantitative support for regional dust risk assessments and policy formulation. Methodologically, it complements long-term model simulations by providing a near-term predictive perspective (Sami et al., 2012).

The forecast results (Fig. 10) indicate that dust radiative forcing over the arid regions of Central Asia during 2024–2029 exhibits an overall quasi-stationary pattern, with interannual fluctuations ranging from 1.6 to $9.8\,\mathrm{W\,m^{-2}}$ (peaking in 2026) and no indications of extreme events. Regional differences are pronounced: southern Xinjiang represents a strong radiative response zone (2.8–$18.9\,\mathrm{W\,m^{-2}}$), whereas northern Xinjiang shows a non-stationary trend of initial increase followed by decline (1.6–$10.0\,\mathrm{W\,m^{-2}}$), likely reflecting the bidirectional modulation of dust emissions by changes in snow cover.

Model validation results (Fig. S11) confirm that the residuals of the $\mathrm{SARIMA}(1,1,0)\times(1,0,2)_{12}$ model satisfy the white noise assumption (Ljung–Box Q test, $p>0.05$) and approximate normality (Kolmogorov–Smirnov test, $D=0.12$), with autocorrelation coefficients falling within the 95 % confidence interval. Quantitative metrics of predictive performance include $\mathrm{RMSE}=1.72\,\mathrm{W\,m^{-2}}$, $\mathrm{MAE}=1.21\,\mathrm{W\,m^{-2}}$, $\mathrm{MAPE}=8.6\,\%$, and $R^2=0.70$, demonstrating the model's strong capability for short-term predictions.

Thus, the SARIMA model serves as a methodological complement: it not only validates the internal variability captured in reanalysis and observational time series but also provides operational forecasts for near-future regional climate risk management. This short-term predictive approach complements CMIP6 long-term simulations, bridging the gap between large-scale climate projections and near-term adaptation needs.

4.2.2 Uncertainty Analysis

The CMIP6 multi-model ensemble (MME) provides a robust analytical framework for assessing future variations in dust budgets across Central Asia. However, differences among models in dust emission parameterization, particle size distribution, and surface schemes introduce a degree of uncertainty in the simulations. To systematically evaluate these uncertainties and enhance the reliability of the results, this study employs complementary diagnostic approaches that quantify both inter-model variability and biases arising from the statistical downscaling procedure.

To assess inter-model dispersion, dust emissions from each model were compared with MERRA-2 reanalysis data. As shown in Fig. 10a, emission biases of individual models were evaluated using a two-tailed t-test ($p<0.05$) to determine statistical significance. The results indicate that several models – including CESM2, CESM2-WACCM, CNRM-ESM2-1, and MRI-ESM2-1 – exhibit relatively large devia-

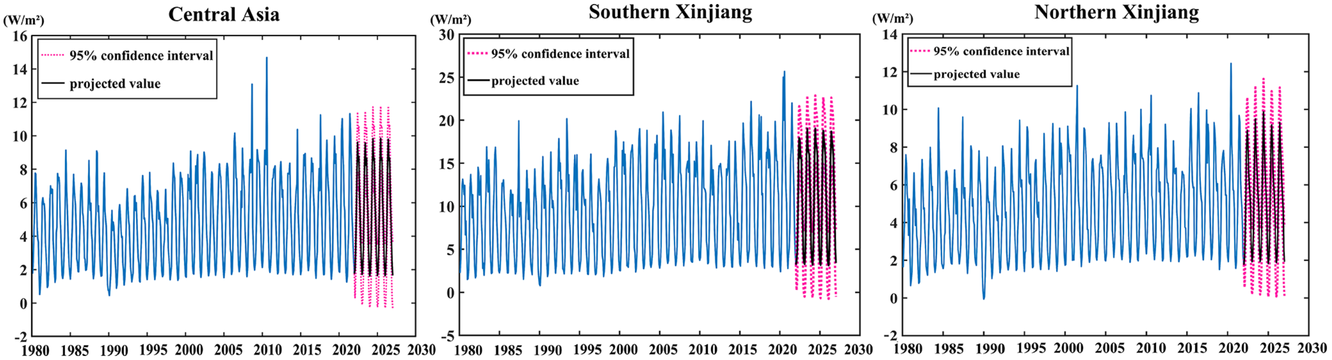

Figure 10. Dust aerosol direct radiative forcing SARIMA model predictions.

tions, suggesting that their dust modules or physical parameterization schemes may introduce additional uncertainties. Figure 10b further illustrates the time series of dust emissions along with the $\pm 1\sigma$ inter-model variability (shaded area). Despite the dispersion among models, the MERRA-2 record consistently falls within the historical model range, indicating that the MME ensemble mean provides a reasonable representation of the climatological mean state and effectively captures the "three-source, high-emission" spatial pattern characteristic of Central Asia's major dust source regions.

To further elucidate regional differences, Figs. 11a and S12 depict the spatial bias distributions of individual models within the multi-model ensemble (MME). The results reveal that all models exhibit biases in key dust source regions, including the Taklamakan Desert, Kumtag Desert, areas surrounding the Aral Sea, Karakum Desert, and the eastern Caspian Sea. Specifically, positive biases predominate in the southeastern Tarim Basin, whereas negative biases dominate in the western Karakum Desert and parts of the Aral Sea region.

The bias-corrected statistical downscaling method employed in this study, which relies on MERRA-2 data, is well-suited to Central Asia's complex terrain and sparse observational networks. It offers low computational costs while preserving the statistical relationships between dust emissions and climate variables. However, its capacity to simulate extreme events and nonlinear processes (e.g., intense dust storms) remains limited.To quantify downscaling biases, Fig. 12b illustrates the spatial root-mean-square error (RMSE) between CMIP6 downscaled outputs and MERRA-2 data. The results indicate higher RMSE values ($> 2\,\mu\mathrm{g\,m^{-2}\,s^{-1}}$) in complex terrain regions, such as the Tarim Basin and Karakum Desert, suggesting that predictions in these areas should be interpreted with caution. Figure S13 presents a scatterplot demonstrating a high correlation between downscaled MME changes (ΔMME) and MERRA-2 observations ($R^2 > 0.91$), although a slight underestimation bias is evident (Bias $= -1.26$, RMSE $= 4.31$). The time series comparison in Fig. S13b further demonstrates that the downscaled results effectively capture seasonal and interannual variability.Overall, the multi-model ensemble, combined with bias-corrected downscaling, demonstrates reasonable robustness, providing a credible reference for assessing future dust changes in Central Asia.

Although the results presented above provide multiple lines of evidence for understanding the dust cycle in Central Asia, their limitations cannot be overlooked. The dust budget encompasses key processes such as emission, transport, deposition, and mass loading. While previous studies have advanced our knowledge, achieving a comprehensive understanding of the complex interactions among dust, land surface, vegetation, and climate remains a significant challenge. In particular, variability in dust particle size assumptions across CMIP6 models markedly affects simulation consistency (Zhao et al., 2022), thereby increasing uncertainty in representing dust cycle processes.

Second, although existing radiative transfer models such as SBDART are suitable for point-scale simulations, they do not fully account for aerosol–cloud interactions, which are particularly important in regions with high dust concentrations; neglecting this process may introduce biases in radiative forcing estimates. The SBDART simulations in this study rely on a limited set of ground-based observational sites in Central Asia, which, while representative in terms of geographic location and underlying surface types, are sparsely distributed and thus capture only local responses at typical sites rather than spatially averaged effects across the entire region. For example, the Ili Lake site exhibits lower atmospheric heating rates in spring, likely attributable to data scarcity and the shielding effects of complex mountainous terrain, underscoring the challenges of high-altitude observations.

Due to the sparse observational network, no weighting was applied to the sites; instead, they were treated as independent case studies to highlight variability under different environmental conditions. The representativeness of these sites is corroborated by cross-validation with MERRA-2 reanalysis data (Fig. S1); however, they still cannot fully characterize

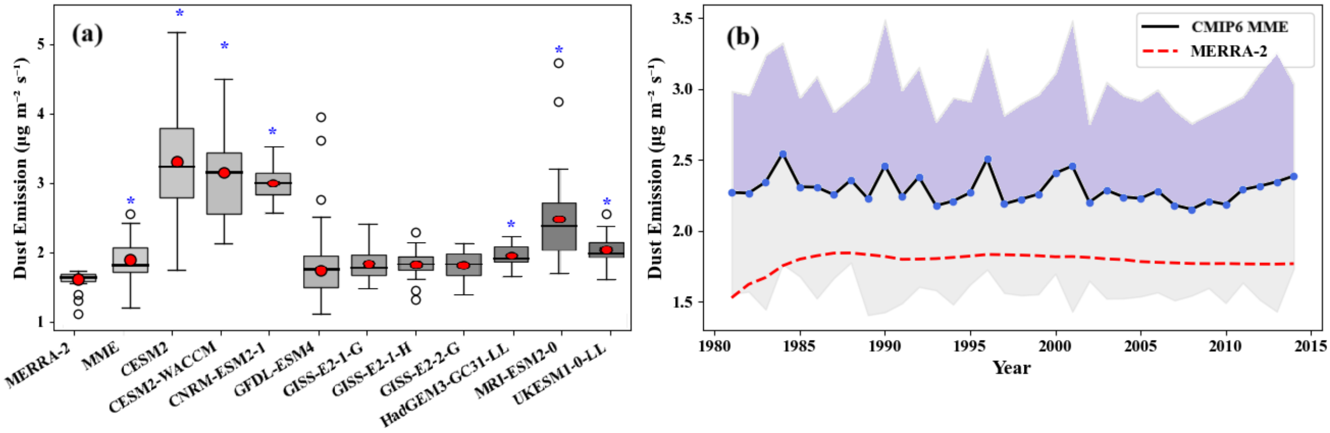

Figure 11. (**a**) Dust emission biases of individual models relative to MERRA-2 reanalysis data; (**b**) time series of dust emissions from the CMIP6 multi-model ensemble, with $\pm 1\sigma$ inter-model variability indicated by the shaded area.

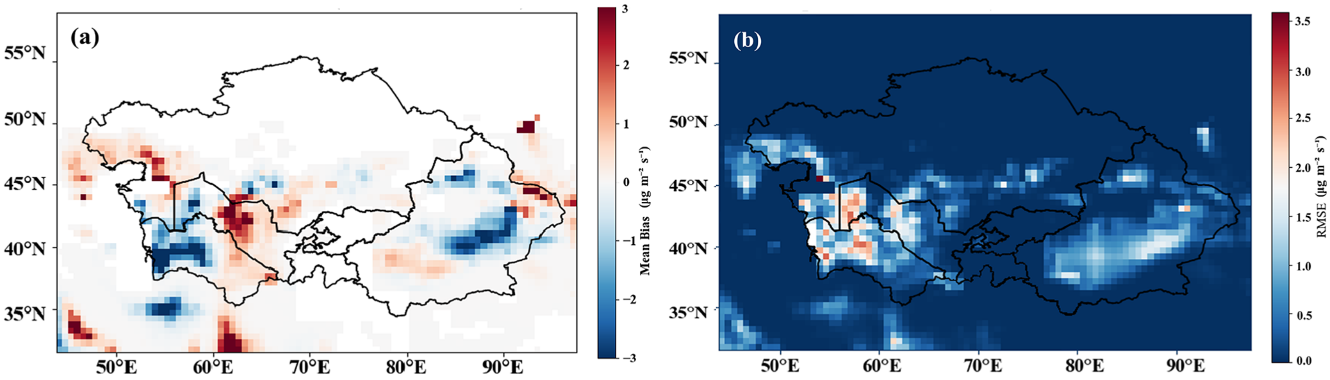

Figure 12. (**a**) Spatial distribution of biases between individual models in the multi-model ensemble and MERRA-2 reanalysis data; (**b**) spatial distribution of root-mean-square error (RMSE) between CMIP6 downscaled outputs and MERRA-2 reanalysis data.

the complex radiative effects across Central Asia's extensive and heterogeneous landscapes.

Code availability. The data analysis and visualization in this study were performed using MATLAB and Python scripts developed by the authors. The scripts used to process and analyze the datasets are available from the corresponding author upon reasonable request.

Data availability. The datasets used in this study are publicly available. MERRA-2 reanalysis data are available from the NASA Global Modeling and Assimilation Office (https://gmao.gsfc.nasa.gov/reanalysis/MERRA-2/, last access: 4 March 2026). CMIP6 model outputs are available through the Earth System Grid Federation (ESGF) data portal (https://esgf-node.llnl.gov/search/cmip6/, last access: 4 March 2026). AERONET aerosol observations are available from the NASA AERONET website (https://aeronet.gsfc.nasa.gov/, last access: 4 March 2026). SONET observations are available from the SONET website (https://spaceclimateobservatory.aerss.net/, last access: 10 March 2026).

Supplement. The supplement related to this article is available online at https://doi.org/10.5194/acp-26-3881-2026-supplement.

Author contributions. All authors contributed to the manuscript and approved the final version. YG designed the study, performed the data analysis, and wrote the original draft. WC, JD, and YR assisted with data collection and software processing. YR also contributed to the validation and interpretation of results. ZZ supervised the research and contributed to manuscript revision and funding acquisition.

Competing interests. The contact author has declared that none of the authors has any competing interests.

text are those of the authors and do not necessarily reflect the views of the publisher.

Special issue statement. This article is part of the special issue "Sun-photometric measurements of aerosols: harmonization, comparisons, synergies, effects, and applications". It is not associated with a conference.

Acknowledgements. The authors thank the science teams of MERRA-2, CMIP6, AERONET, and SONET for providing the datasets used in this study.

Financial support. This research has been supported by the Open Project of Key Laboratory in Xinjiang Uygur Autonomous Region of China (grant no. 2023D04066), the National Natural Science Foundation of China (grant no. 42061066), and the Xinjiang University Outstanding Graduate Student Innovation Program (grant no. XJDX2025YJS065).

Review statement. This paper was edited by Stephanie Fiedler and reviewed by two anonymous referees.

References

Bauer, S. E. and Koch, D.: Impact of heterogeneous sulfate formation at mineral dust surfaces on aerosol loads and radiative forcing in the Goddard Institute for Space Studies general circulation model, J. Geophys. Res.-Atmos., 110, D17202, https://doi.org/10.1029/2005JD005870, 2005.

Bauer, S. E., Tsigaridis, K., Faluvegi, G., Kelley, M., Lo, K. K., Miller, R. L., Nazarenko, L., Schmidt, G. A., and Wu, J.: Historical (1850–2014) aerosol evolution and role on climate forcing using the GISS ModelE2.1 contribution to CMIP6, J. Adv. Model. Earth Sy., 12, e2019MS001978, https://doi.org/10.1029/2019MS001978, 2020.

Braconnot, P., Albani, S., Balkanski, Y., Cozic, A., Kageyama, M., Sima, A., Marti, O., and Peterschmitt, J.-Y.: Impact of dust in PMIP-CMIP6 mid-Holocene simulations with the IPSL model, Clim. Past, 17, 1091–1117, https://doi.org/10.5194/cp-17-1091-2021, 2021.

Brown, H., Liu, X., Pokhrel, R., Murphy, S., Lu, Z., Saleh, R., Mielonen, T., Kokkola, H., Bergman, T., and Myhre, G.: Biomass burning aerosols in most climate models are too absorbing, Nat. Commun., 12, 277, https://doi.org/10.1038/s41467-020-20482-9, 2021.

Buchard, V., Randles, C. A., da Silva, A. M., Darmenov, A., Colarco, P. R., Govindaraju, R., Ferrare, R., Hair, J., Beyersdorf, A. J., and Ziemba, L. D.: The MERRA-2 aerosol reanalysis, 1980 onward. Part II: Evaluation and case studies, J. Climate, 30, 6851–6872, https://doi.org/10.1175/JCLI-D-16-0613.1, 2017.

Cakmur, R. V., Miller, R. L., Perlwitz, J., Geogdzhayev, I. V., Ginoux, P., Koch, D., Kohfeld, K. E., Tegen, I., and Zender, C. S.: Constraining the magnitude of the global dust cycle by minimizing the difference between a model and observations, J. Geophys. Res.-Atmos., 111, D06207, https://doi.org/10.1029/2005JD005791, 2006.

Chen, A., Zhao, C., and Fan, T.: Spatio-temporal distribution of aerosol direct radiative forcing over mid-latitude regions in north hemisphere estimated from satellite observations, Atmos. Res., 266, 105938, https://doi.org/10.1016/j.atmosres.2021.105938, 2022.

Dai, Y., Hitchcock, P., Mahowald, N. M., Domeisen, D. I. V., Hamilton, D. S., Li, L., Marticorena, B., Kanakidou, M., Mihalopoulos, N., and Aboagye-Okyere, A.: Stratospheric impacts on dust transport and air pollution in West Africa and the Eastern Mediterranean, Nat. Commun., 13, 7744, https://doi.org/10.1038/s41467-022-35403-1, 2022.

Danabasoglu, G., Lamarque, J.-F., Bacmeister, J., Bailey, D. A., DuVivier, A. K., Edwards, J., Emmons, L. K., Fasullo, J., Garcia, R., Gettelman, A., Hannay, C., Holland, M., Large, W. G., Lauritzen, P., Lawrence, D., Lenaerts, J. T. M., Lindsay, K., Lipscomb, W., Mills, M., Neale, R., Oleson, K., Otto-Bliesner, B., Phillips, A., Sacks,W., Tilmes, S., van Kampenhout, L., Vertenstein, M., Bertini, A., Dennis, J., Deser, C., Fischer, C., Fox-Kemper, B., Kay, J., Kinnison, D., Kushner, P., Larson, V., Long, M., Mickelson, S., Moore, J., Nienhouse, E., Polvani, L., Rasch, P., and Strand, G.: The Community Earth System Model Version 2 (CESM2), J. Adv. Model. Earth Sy., 12, e2019MS001916, https://doi.org/10.1029/2019MS001916, 2020.

Dubovik, O. and King, M. D.: A flexible inversion algorithm for retrieval of aerosol optical properties from Sun and sky radiance measurements, J. Geophys. Res.-Atmos., 105, 20673–20696, https://doi.org/10.1029/2000JD900282, 2000.

Dunne, J. P., Horowitz, L. W., Adcroft, A. J., Ginoux, P., Held, I. M., John, J. G., Krasting, J. P., Malyshev, S., Naik, V., Paulot, F., Shevliakova, E., Stock, C. A., Zadeh, N., Balaji, V., Blanton, C., Dunne, K. A., Dupuis, C., Durachta, J., Dussin, R., Gauthier, P. P. G., Griffies, S. M., Guo, H., Hallberg, R. W., Harrison, M., He, J., Hurlin, W., McHugh, C., Menzel, R., Milly, P. C. D., Nikonov, S., Paynter, D. J., Ploshay, J., Radhakrishnan, A., Rand, K., Reichl, B. G., Robinson, T., Schwarzkopf, D. M., Sentman, L. T., Underwood, S., Vahlenkamp, H., Winton, M., Wittenberg, A. T., Wyman, B., Zeng, Y., and Zhao, M.: The GFDL Earth System Model Version 4.1 (GFDL728 ESM4.1): Overall coupled model description and simulation characteristics, J. Adv. Model. Earth Sy., 12, e2019MS002015, https://doi.org/10.1029/2019MS002015, 2020.

Evans, S., Ginoux, P., Malyshev, S., and Shevliakova, E.: Climate–vegetation interaction and amplification of Australian dust variability, Geophys. Res. Lett., 43, 11823–11830, https://doi.org/10.1002/2016GL071016, 2016.

Eyring, V., Bony, S., Meehl, G. A., Senior, C. A., Stevens, B., Stouffer, R. J., and Taylor, K. E.: Overview of the Coupled Model Intercomparison Project Phase 6 (CMIP6) experimental design and organization, Geosci. Model Dev., 9, 1937–1958, https://doi.org/10.5194/gmd-9-1937-2016, 2016.

Fu, A., Li, W., Chen, Y., Wang, Y., Hao, H., Li, Y., Sun, F., Zhou, H., Zhu, C., and Hao, X.: The effects of ecological rehabilitation projects on the resilience of an extremely drought-prone desert riparian forest ecosystem in the Tarim River Basin, Xinjiang, China, Sci. Rep., 11, 18485, https://doi.org/10.1038/s41598-021-96742-5, 2021.

García, O. E., Díaz, J. P., Expósito, F. J., Díaz, A. M., Dubovik, O., Derimian, Y., Dubuisson, P., and Roger, J.-C.: Shortwave radiative forcing and efficiency of key aerosol types using AERONET data, Atmos. Chem. Phys., 12, 5129–5145, https://doi.org/10.5194/acp-12-5129-2012, 2012.

Gelaro, R., McCarty, W., Suárez, M. J., Todling, R., Molod, A., Takacs, 745 L., Randles, C. A., Darmenov, A., Bosilovich, M. G., Reichle, R., Wargan, K., Coy, L., Cullather, R., Draper, C., Akella, S., Buchard, V., Conaty, A., da Silva, A. M., Gu, W., Kim, G.-K., Koster, R., Lucchesi, R., Merkova, D., Nielsen, J. E., Partyka, G., Pawson, S., Putman, W., Rienecker, M., Schubert, S. D., Sienkiewicz, M., and Zhao, B.: The Modern-Era Retrospective Analysis for Research and Applications, version 2 (MERRA-2), J. Climate, 30, 5419–5454, https://doi.org/10.1175/JCLI-D-16-0758.1, 2017.

Ginoux, P., Prospero, J. M., Gill, T. E., Hsu, N. C., and Zhao, M.: Global-scale attribution of anthropogenic and natural dust sources and their emission rates based on MODIS Deep Blue aerosol products, Rev. Geophys., 50, RG3005, https://doi.org/10.1029/2012RG000388, 2012.

Gutmann, E., Pruitt, T., Clark, M. P., Brekke, L., Arnold, J. R., Raff, D. A., and Rasmussen, R. M.: An intercomparison of statistical downscaling methods used for water resource assessments in the United States, Water Resour. Res., 50, 7167–7186, https://doi.org/10.1002/2014WR015559, 2014.

Halthore, R. N., Crisp, D., Schwartz, S. E., Anderson, G. P., Berk, A., Bonnel, B., Boucher, O., 759 Chang, F.-L., Chou, M.-D., Clothiaux, E. E., Dubuisson, P., Fomin, B., Fouquart, Y., Freidenreich, S., Gautier, C., Kato, S., Laszlo, I., Li, Z., Mather, J. H., Plana-Fattori, A., Ramaswamy, V., Ricchiazzi, P., Shiren, Y., Trishchenko, A., and Wiscombe, W.: Intercomparison of shortwave radiative transfer codes and measurements, J. Geophys. Res.-Atmos., 110, D11206, https://doi.org/10.1029/2004JD005293, 2005.

Hetzel, R., Niedermann, S., Tao, M., Kubik, P. W., Ivy-Ochs, S., Gao, B., and Strecker, M. R.: Low slip rates and long-term preservation of geomorphic features in Central Asia, Nature, 417, 428–432, https://doi.org/10.1038/417428a, 2002.

Holben, B. N., Eck, T. F., Slutsker, I., Tanré, D., Buis, J. P., Setzer, A., Vermote, E., Reagan, J. A., Kaufman, Y. J., Nakajima, T., Lavenu, F., Jankowiak, I., and Smirnov, A.: AERONET – A federated instrument network and data archive for aerosol characterization, Remote Sens. Environ., 66, 1–16, https://doi.org/10.1016/S0034-4257(98)00031-5, 1998.

Holben, B. N., Tanré, D., Smirnov, A., Eck, T. F., Slutsker, I., Abuhassan, N., Newcomb, W. W., Schafer, J. S., Chatenet, B., Lavenu, F., Kaufman, Y. J., Castle, J., Setzer, A., Markham, B., Clark, D., Frouin, R., Halthore, R., Karneli, A., O'Neill, N. T., Pietras, C., Pinker, R. T., Voss, K., and Zibordi, G.: An emerging ground-based aerosol climatology: Aerosol optical depth from AERONET, J. Geophys. Res.-Atmos., 106, 12067–12097, https://doi.org/10.1029/2001JD900014, 2001.

IPCC: Climate Change 2021: The Physical Science Basis. Contribution of Working Group I to the Sixth Assessment Report of the Intergovernmental Panel on Climate Change, edited by: Masson-Delmotte, V., Zhai, P., Pirani, A., Connors, S. L., Péan, C., Berger, S., Caud, N., Chen, Y., Goldfarb, L., Gomis, M. I., Huang, M., Leitzell, K., Lonnoy, E., Matthews, J. B. R., Maycock, T. K., Waterfield, T., Yelekçi, O., Yu, R., and Zhou, B., Cambridge University Press, Cambridge, United Kingdom and New York, NY, USA, 2391 pp., https://doi.org/10.1017/9781009157896, 2021.

Kok, J. F., Ridley, D. A., Zhou, Q., Miller, R. L., Zhao, C., Heald, C. L., Ward, D. S., Albani, S., and Haustein, K.: Smaller desert dust cooling effect estimated from analysis of dust size and abundance, Nat. Geosci., 10, 274–278, https://doi.org/10.1038/ngeo2912, 2017.

Kok, J. F., Storelvmo, T., Karydis, V. A., Adebiyi, A. A., Mahowald, N. M., Evan, A. T., He, C., and Leung, D. M.: Mineral dust aerosol impacts on global climate and climate change, Nat. Rev. Earth Environ., 4, 71–86, https://doi.org/10.1038/s43017-022-00379-5, 2023.

Kumar, M., Parmar, K. S., Kumar, D. B., Mhawish, A., Broday, D. M., Mall, R. K., and Banerjee, T.: Long-term aerosol climatology over Indo-Gangetic plain: trend, prediction and potential source fields, Atmos. Environ., 180, 37–50, https://doi.org/10.1016/j.atmosenv.2018.02.027, 2018.

Kelley, M., Schmidt, G. A., Nazarenko, L., Miller, R. L., Bauer, S. E., Ruedy, R., Russell, G. L., Ackerman, A. S., Aleinov, I., Bauer, M., Bleck, R., Canuto, V., Cesana, G., Cheng, Y., Clune, T. L., Cook, B. I., Cruz, C. A., Del Genio, A. D., Elsaesser, G. S., Faluvegi, G., Kiang, N. Y., Kim, D., Lacis, A. A., Leboissetier, A., LeGrande, A. N., Lo, K. K., Marshall, J., Matthews, E. E., McDermid, S., Mezuman, K., Murray, L. T., Oinas, V., Orbe, C., García-Pando, C. P., Perlwitz, J. P., Puma, M. J., Rind, D., Romanou, A., Shindell, D. T., Sun, S., Tausnev, N., Tsigaridis, K., Tselioudis, G., Weng, E., Wu, J., and Yao, M.-S.: GISS-E2.1: Configurations and climatology, J. Adv. Model. Earth Sy., 12, e2019MS002025, https://doi.org/10.1029/2019MS002025, 2020.

Kuhlbrodt, T., Jones, C. G., Sellar,A., Storkey, D., Blockley, E., Stringer, M., Hill, R., Graham, T., Ridley, J., Blaker,A., Calvert, D., Copsey, D., Ellis, R., Hewitt, H., Hyder, P., Ineson, S., Mulcahy, J., Siahaan, A., and Walton, J.: The low-resolution version of HadGEM3 GC3.1: Development and evaluation for global climate, J. Adv. Model. Earth Sy., 10, 2865–2888, https://doi.org/10.1029/2018MS001370, 2018.

Li, J., Carlson, B. E., Yung, Y. L., Lv, D., Hansen, J., Penner, J. E., Liao, H., Ramaswamy, V., Kahn, R. A., Zhang, P., Dubovik, O., Ding, A., Lacis, A. A., Zhang, L., and Dong, Y.: Scattering and absorbing aerosols in the climate system, Nat. Rev. Earth Environ., 3, 363–379, https://doi.org/10.1038/s43017-022-00296-7, 2022a.

Li, X., Dong, X., Liu, Y., Wang, M., Jiang, Y., and Dong, Y.: Assessment of the Coupled Model Intercomparison Project phase 6 (CMIP6) model performance in simulating the spatial-temporal variation of aerosol optical depth over Eastern Central China, Atmos. Res., 261, 105747, https://doi.org/10.1016/j.atmosres.2021.105747, 2021.

Li, Y., Song, Y., Kaskaoutis, D. G., Zhang, X., Chen, X., Shukurov, N., and Orozbaev, R.: Atmospheric dust dynamics over Central Asia: A perspective view from loess deposits, Gondwana Res., 109, 150–165, https://doi.org/10.1016/j.gr.2022.04.019, 2022b.

Li, Z., Xu, H., Li, K. T., Li, D., Xie, Y., Li, L., Zhang, Y., Gu, X., Zhao,W., Tian, Q., Deng, R., Su, Y., Huang, B., Cui, W., Deng, X., Hu, B., Cui, Y., and Zhang, X.: Comprehensive study of optical, physical, chemical, and radiative properties of total columnar atmospheric aerosols over China: An overview of Sun–Sky Radiometer Observation Network (SONET) measurements, B. Am. Meteorol. Soc., 99, 739–755, https://doi.org/10.1175/BAMS-D-17-0133.1, 2018.

Lioubimtseva, E. and Cole, R.: Uncertainties of climate change in arid environments of Central Asia, Rev. Fish. Sci., 14, 29–49, https://doi.org/10.1080/10641260500340603, 2006.

Liu, J., Wang, X., Wu, D., Wei, H., Li, Y., and Ji, M.: Historical footprints and future projections of global dust burden from bias-corrected CMIP6 models, npj Clim. Atmos. Sci., 7, 1, https://doi.org/10.1038/s41612-023-00550-9, 2024.

Mahowald, N. M., Kloster, S., Engelstaedter, S., Moore, J. K., Mukhopadhyay, S., McConnell, J. R., Albani, S., Doney, S. C., Bhattacharya, A., Curran, M. A. J., Flanner, M. G., Hoffman, F. M., Lawrence, D. M., Lindsay, K., Mayewski, P. A., Neff, J., Rothenberg, D., Thomas, E., Thornton, P. E., and Zender, C. S.: Observed 20th century desert dust variability: impact on climate and biogeochemistry, Atmos. Chem. Phys., 10, 10875–10893, https://doi.org/10.5194/acp-10-10875-2010, 2010.

Maraun, D., Wetterhall, F., Ireson, A. M., Chandler, R. E., Kendon, E. J., Widmann, M., Brienen, S., Rust, H. W., Sauter, T., Themeßl, M., and Thiele-Eich, I.: Precipitation downscaling under climate change: Recent developments to bridge the gap between dynamical models and the end user, Rev. Geophys., 48, RG3003, https://doi.org/10.1029/2009RG000314, 2010.

Marticorena, B. and Bergametti, G.: Modeling the atmospheric dust cycle: 1. Design of a soil-derived dust emission scheme, J. Geophys. Res.-Atmos., 100, 16415–16430, https://doi.org/10.1029/95JD00690, 1995.

Marticorena, B., Bergametti, G., Aumont, B., Callot, Y., N'Doumé, C., and Legrand, M.: Modeling the atmospheric dust cycle: 2. Simulation of Saharan dust sources, J. Geophys. Res.-Atmos., 102, 4387–4404, https://doi.org/10.1029/96JD02964, 1997.

Miller, R. L., Tegen, I., and Perlwitz, J.: Surface radiative forcing by soil dust aerosols and the hydrologic cycle, J. Geophys. Res.-Atmos., 109, D04203, https://doi.org/10.1029/2003JD004085, 2004.

Nakamae, K. and Takemi, T.: Relationship between the development of a convective mixed layer and dust weather in arid and semi-arid regions of East Asia, Int. J. Climatol., 42, 3076–3093, https://doi.org/10.1002/joc.7373, 2022.

Penner, J. E., Quaas, J., Storelvmo, T., Takemura, T., Boucher, O., Guo, H., Kirkevåg, A., Kristjánsson, J. E., and Seland, Ø.: Model intercomparison of indirect aerosol effects, Atmos. Chem. Phys., 6, 3391–3405, https://doi.org/10.5194/acp-6-3391-2006, 2006.

Pozzer, A., de Meij, A., Pringle, K. J., Tost, H., Doering, U. M., van Aardenne, J., and Lelieveld, J.: Distributions and regional budgets of aerosols and their precursors simulated with the EMAC chemistry-climate model, Atmos. Chem. Phys., 12, 961–987, https://doi.org/10.5194/acp-12-961-2012, 2012.

Rind, D., Orbe, C., Jonas, J., Nazarenko, L., Zhou, T., Kelley, M., Lacis, A., Shindell, D., Faluvegi, G., Russell, G., Bauer, M., Schmidt, G., Romanou, A., and Tausnev, N.: GISS ModelE2.2: A climate model optimized for the middle atmosphere–Model structure, climatology, variability, and climate sensitivity, J. Geophys. Res.-Atmos., 125, e2019JD032204, https://doi.org/10.1029/2019JD032204, 2020.

Rupakheti, D., Rupakheti, M., Rai, M., Yin, X., Hofer, J., Hu, Y., Abdullaev, S. F., Kang, S., and Lawrence, M. G.: Characterization of columnar aerosol over a background site in Central Asia, Environ. Pollut., 316, 120501, https://doi.org/10.1016/j.envpol.2022.120501, 2023.

Ramanathan, V., Crutzen, P. J., Kiehl, J. T., and Rosenfeld, D.: Aerosols, climate, and the hydrological cycle, Science, 294, 2119–2124, https://doi.org/10.1126/science.1064034, 2001.

Ricchiazzi, P., Yang, S., Gautier, C., and Sowle, D.: SBDART: A research and teaching software tool for plane-parallel radiative transfer in the Earth's atmosphere, B. Am. Meteorol. Soc., 79, 2101–2114, https://doi.org/10.1175/1520-0477(1998)079<2101:SARATS>2.0.CO;2, 1998.

Salvador, P., Pey, J., Pérez, N., Querol, X., and Artíñano, B.: Increasing atmospheric dust transport towards the western Mediterranean over 1948–2020, npj Clim. Atmos. Sci., 5, 34, https://doi.org/10.1038/s41612-022-00255-9, 2022.

Sami, M., Waseem, A., Jafri, Y. Z., Shah, S. H., Khan, M. A., Akbar, S., Siddiqui, M. A., and Murtaza, G.: Prediction of the rate of dust fall in Quetta city, Pakistan using seasonal ARIMA (SARIMA) modeling, Int. J. Phys. Sci., 7, 1713–1725, https://doi.org/10.5897/IJPS11.1357, 2012.

Séférian, R., Nabat, P., Michou, M., Saint-Martin, D., Voldoire, A., Colin, J., Decharme, B., Delire, C., Berthet, S., Chevallier, M., Sénési, S., Franchisteguy, L., Vial, J., Mallet, M., Joetzjer, E., Geoffroy, O., Guérémy, J.-F., Moine, M.-P., Msadek, R., Ribes, A., Rocher, M., Roehrig, R., Salas y-Mélia, D., Sanchez, E., Terray, L., Valcke, S., Waldman, R., Aumont, O., Bopp, L., Deshayes, J., Éthé, C., and Madec, G.: Evaluation of the CNRM Earth System Model (CNRM-ESM2-1): Role of Earth system processes in present-day and future climate, J. Adv. Model. Earth Sy., 11, 4182–4227, https://doi.org/10.1029/2019MS001791, 2019.

Senior, C. A., Jones, C. G., Wood, R. A., Sellar,A., Belcher, S., Klein-Tank, A., Sutton, R., Walton, J., Lawrence, B., Andrews, T., and Mulcahy, J. P.: U.K. community Earth system modeling for CMIP6, J. Adv. Model. Earth Sy., 12, e2019MS002004, https://doi.org/10.1029/2019MS002004, 2020.

Shao, Y., Wyrwoll, K.-H., Chappell, A., Huang, J., Lin, Z., McTainsh, G. H., Mikami, M., Tanaka, T. Y., Wang, X., and Yoon, S.: Dust cycle: An emerging core theme in Earth system science, Aeolian Res., 2, 181–204, https://doi.org/10.1016/j.aeolia.2011.02.001, 2011.

She, L., Li, Z., de Leeuw, G., Wang, Y., Wang, L., Yang, Z., Feng, C., Yang, C., and Shi, Y.: Time series retrieval of multi-wavelength aerosol optical depth by adapting Transformer (TMAT) using Himawari-8 AHI data, Remote Sens. Environ., 305, 114115, https://doi.org/10.1016/j.rse.2024.114115, 2024.

Shen, H., Abuduwaili, J., Samat, A., and Ma, L.: A review on the research of modern aeolian dust in Central Asia, Arab. J. Geosci., 9, 326, https://doi.org/10.1007/s12517-016-2646-9, 2016.

Sirisha, U. M., Belavagi, M. C., and Attigeri, G.: Profit prediction using ARIMA, SARIMA and LSTM models in time series forecasting: A comparison, IEEE Access, 10, 124715–124727, 2022.

Song, Q., Zhang, Z., Yu, H., Ginoux, P., and Shen, J.: Global dust optical depth climatology derived from CALIOP and MODIS aerosol retrievals on decadal timescales: regional and interannual variability, Atmos. Chem. Phys., 21, 13369–13395, https://doi.org/10.5194/acp-21-13369-2021, 2021.

Tanaka, T. Y. and Chiba, M.: A numerical study of the contributions of dust source regions to the global dust budget, Global Planet. Change, 52, 88–104, https://doi.org/10.1016/j.gloplacha.2006.02.002, 2006.

Tao, M., Chen, L., Wang, J., Wang, L., Wang, W., Lin, C., Gui, L., Wang, C., Yu, C., and Wang, Y.: Characterization of dust activation and their prevailing transport over East Asia based on multi-satellite observations, Atmos. Res., 265, 105886, https://doi.org/10.1016/j.atmosres.2021.105886, 2022.

Tegen, I., Werner, M., Harrison, S. P., and Kohfeld, K. E.: Relative importance of climate and land use in determining present and future global soil dust emission, Geophys. Res. Lett., 31, L05105, https://doi.org/10.1029/2003GL019216, 2004.

Wallace, J. M. and Hobbs, P. V.: Atmospheric science: an introductory survey, 2nd edn., Academic Press, Amsterdam, 483 pp., ISBN 978-0-12-732951-2, 2006.

Wang, X., Liu, J., Che, H., Ji, F., and Liu, J.: Spatial and temporal evolution of natural and anthropogenic dust events over northern China, Sci. Rep., 8, 2141, https://doi.org/10.1038/s4159838-018-20382-5, 2018.

Wang, X., Chen, Y., Li, Z., Fang, G., Wang, F., and Liu, H.: The impact of climate change and human activities on the Aral Sea Basin over the past 50 years, Atmos. Res., 245, 105125, https://doi.org/10.1016/j.atmosres.2020.105125, 2020.

Wu, C., Lin, Z., He, J., Zhang, M., Liu, X., Zhang, R., and Brown, H.: A process-oriented evaluation of dust emission parameterizations in CESM: Simulation of a typical severe dust storm in East Asia, J. Adv. Model. Earth Sy., 8, 1432–1452, https://doi.org/10.1002/2016MS000723, 2016.

Wu, T. and Boor, B. E.: Urban aerosol size distributions: a global perspective, Atmos. Chem. Phys., 21, 8883–8914, https://doi.org/10.5194/acp-21-8883-2021, 2021.

Xu, M., Wang, X., Sun, T., Wu, H., Li, X., and Kang, S.: Water balance change and its implications to vegetation in the Tarim River Basin, Central Asia, Quatern. Int., 523, 25–36, https://doi.org/10.1016/j.quaint.2019.05.008, 2019.

Yukimoto, S., Koshiro, T., Kawai, H., Oshima, N., Yoshida, K., Urakawa, S., Tsujino, H., Deushi, M., Tanaka, T., Hosaka, M., Yoshimura, H., Shindo, E., Mizuta, R., Ishii, M., Obata, A., and Adachi, Y.: The Meteorological Research Institute Earth System Model Version 2.0, MRI-ESM2.0: Description and basic evaluation of the physical component, J. Meteorol. Soc. Jpn., 97, 931–965, https://doi.org/10.2151/jmsj.2019-051, 2019.

Zender, C. S., Bian, H., and Newman, D.: Mineral Dust Entrainment and Deposition (DEAD) model: Description and 1990s dust climatology, J. Geophys. Res.-Atmos., 108, 4416, https://doi.org/10.1029/2002JD002775, 2003.

Zhang, X.-X., Claiborn, C., Lei, J.-Q., Vaughan, J., Wu, S.-X., Li, S.-Y., Liu, L.-Y., Wang, Z.-F., Wang, Y.-D., Huang, S.-Y., and Li, J.: Aeolian dust in Central Asia: spatial distribution and temporal variability, Atmos. Environ., 238, 117734, https://doi.org/10.1016/j.atmosenv.2020.117734, 2020.

Zhao, A., Ryder, C. L., and Wilcox, L. J.: How well do the CMIP6 models simulate dust aerosols?, Atmos. Chem. Phys., 22, 2095–2119, https://doi.org/10.5194/acp-22-2095-2022, 2022.

Zhao, A., Wilcox, L. J., and Ryder, C. L.: The key role of atmospheric absorption in the Asian summer monsoon response to dust emissions in CMIP6 models, Atmos. Chem. Phys., 24, 13385–13402, https://doi.org/10.5194/acp-24-13385-2024, 2024.

Zhao, Y., Yue, X., Cao, Y., Zhu, J., Tian, C., Zhou, H., Chen, Y., Hu, Y., Fu, W., and Zhao, X.: Multi-model ensemble projection of the global dust cycle by the end of 21st century using the Coupled Model Intercomparison Project version 6 data, Atmos. Chem. Phys., 23, 7823–7838, https://doi.org/10.5194/acp-23-7823-2023, 2023.